nature cell biology

Protein interaction switches coordinate Raf-1 and MST2/Hippo signalling

David Romano[1], Lan K. Nguyen[1], David Matallanas[1], Melinda Halasz[1], Carolanne Doherty[1], Boris N. Kholodenko[1,2,3,4,5] and Walter Kolch[1,2,3,4,5]

Signal transduction requires the coordination of activities between different pathways. In mammalian cells, Raf-1 regulates the MST–LATS and MEK–ERK pathways. We found that a complex circuitry of competing protein interactions coordinates the crosstalk between the ERK and MST pathways. Combining mathematical modelling and experimental validation we show that competing protein interactions can cause steep signalling switches through phosphorylation-induced changes in binding affinities. These include Akt phosphorylation of MST2 and a feedback phosphorylation of Raf-1 Ser 259 by LATS1, which enables Raf-1 to suppress both MST2 and MEK signalling. Mutation of Raf-1 Ser 259 stimulates both pathways, simultaneously driving apoptosis and proliferation, whereas concomitant MST2 downregulation switches signalling to cell proliferation, transformation and survival. Thus, competing protein interactions provide a versatile regulatory mechanism for signal distribution through the dynamic integration of graded signals into switch-like responses.

We are uncovering increasingly complex protein networks that process signals that specify biological responses. Fundamental questions emerge even from small network modules where one protein can have several functions, and where similar configurations can determine different responses[1,2]. For instance, a fundamental question is how signalling networks generate specific decisions. In the ERK pathway, different activation kinetics can determine different cell fates[3]. This kinetic information is decoded into differential biochemical responses by the differential stabilization or activation of transcription factors[4,5], or the assembly of different protein complexes[6]. However, how these mutually exclusive responses are coordinated is unknown. Here, we address this question investigating the coordination of the mammalian MEK–ERK and MST2 pathways by Raf-1.

Raf-1 controls cell proliferation, oncogenic transformation, differentiation and apoptosis. Many of these effects are transmitted by a three-tiered kinase cascade, where Raf-1 phosphorylates and activates MEK, which then phosphorylates and activates ERK. Raf-1 activation ensues by binding to activated Ras proteins, which triggers dephosphorylation of the inhibitory phosphorylated Ser 259 (pS259) and phosphorylation of the activating Ser 338 sites in Raf-1 (refs 7,8). Furthermore, Raf-1 controls apoptosis and cell migration independently of ERK by inhibiting ASK1 (ref. 9), MST2 (ref. 10) and ROKα (ref. 11). These functions are also independent of Raf-1 kinase activity, but reliant on Raf-1 interacting with its targets. For instance, Raf-1 binding to MST2 interferes with MST2 dimerization and activation[10]. MST2 is a mammalian orthologue of Hippo, a *Drosophila* kinase, which governs cell proliferation, growth and apoptosis[12] by activating LATS (ref. 13). Raf-1-mediated MST2 inhibition is relieved by RASSF1A (ref. 14), a tumour suppressor frequently silenced in human cancers[15,16]. In addition, Akt phosphorylates MST2 inhibiting MST2 activity and RASSF1A binding[17].

The observation that Raf-1 and RASSF1A compete for MST2 binding[14] suggested that competing protein interactions may be a mechanism for coordinating the activities of the MST2 and ERK pathways in mammalian cells. Notably, a direct crosstalk between these pathways has not been observed in genetic studies in *Drosophila*, probably because the *Drosophila* Raf orthologue corresponds to B-Raf, which does not bind to and control MST2 (ref. 10), and because MST2 regulation is different in mammalian cells[12,18,19].

RESULTS

Crosstalk between MST2 and ERK pathways

To investigate whether Raf-1 regulation of the ERK and MST2 pathways is coordinated, we stimulated cells with serum and examined the composition of Raf-1 complexes and MST2 and ERK activation kinetics (Fig. 1a). Serum induced a sharp transition from Raf-1–

[1]Systems Biology Ireland, University College Dublin, Dublin 4, Ireland. [2]Conway Institute of Biomolecular & Biomedical Research, University College Dublin, Dublin 4, Ireland. [3]School of Medicine and Medical Sciences, University College Dublin, Dublin 4, Ireland. [4]These authors jointly supervised this work.
[5]Correspondence should be addressed to B.N.K. or W.K. (e-mail: boris.kholodenko@ucd.ie or walter.kolch@ucd.ie)

Received 17 December 2013; accepted 8 May 2014; published online 15 June 2014; DOI: 10.1038/ncb2986

© 2014 Macmillan Publishers Limited. All rights reserved.

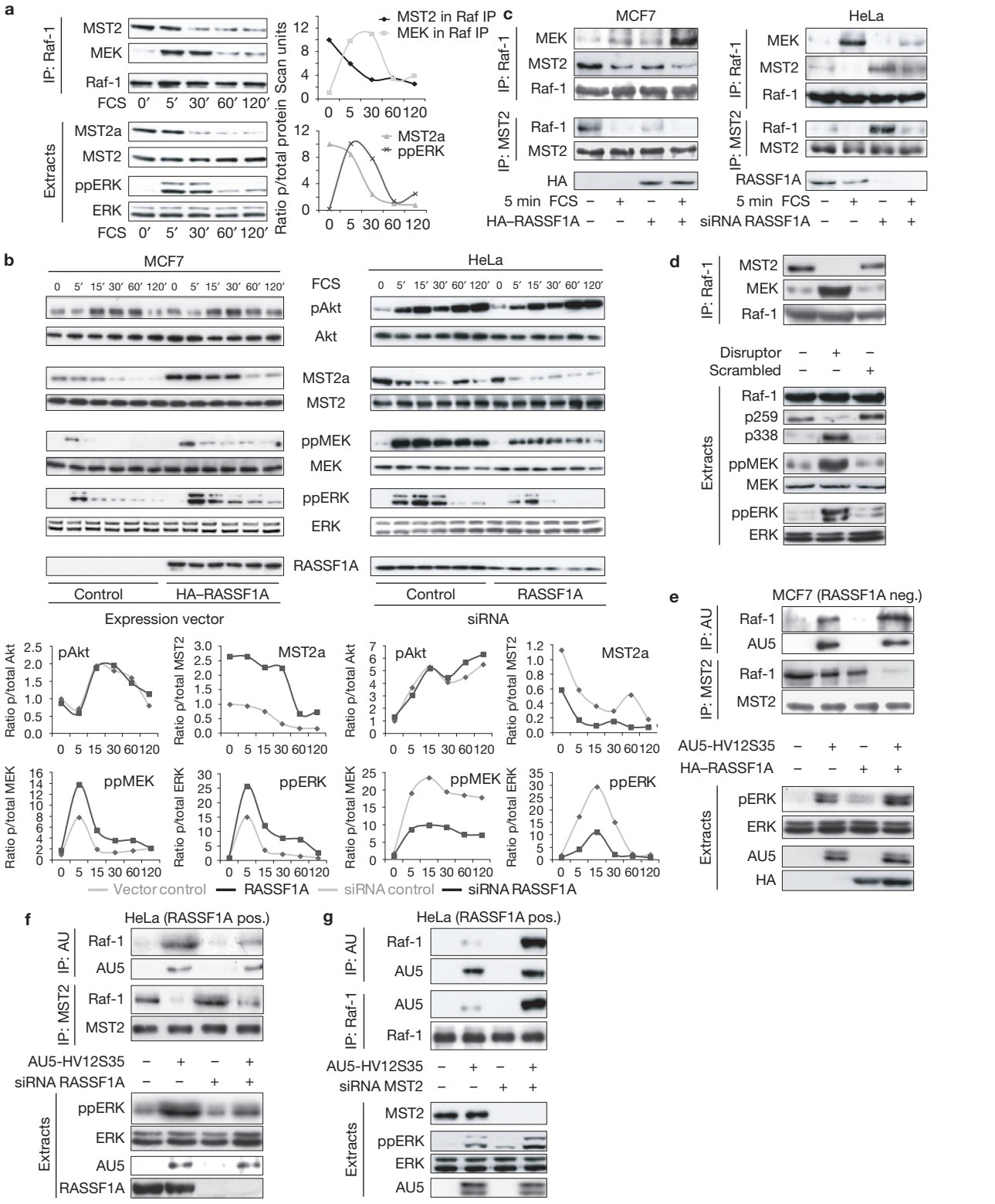

Figure 1 Crosstalk between MST2 and ERK pathways. Cells were transfected, serum starved, and stimulated with 10% serum (FCS) as indicated. Extracts and immunoprecipitates (IPs) were analysed by immunoblotting. (**a**) MST2 and MEK binding to Raf-1, and MST2 and ERK activation in HeLa cells. (**b**,**c**) Cells were transfected with a HA–RASSF1A expression vector or RASSF1A siRNA, and assessed for Akt, MST2, MEK, ERK activation (**b**), or Raf-1 and MST2 association (**c**). MCF7 cells lack endogenous RASSF1A expression. (**d**) HeLa cells were incubated with stearoylated-MST2 (Disruptor) or scrambled control peptides. Raf-1 immunoprecipitates were blotted for associated MST2 and MEK. (**e**–**g**) Cells were transfected as indicated. AU5-RasV12S35, MST2 and Raf-1 immunoprecipitates were analysed for changes in co-immunoprecipitating proteins. Uncropped images of blots are shown in Supplementary Fig. 6.

© 2014 Macmillan Publishers Limited. All rights reserved.

MST2 to Raf-1–MEK binding, which was accompanied by a sharp decrease in MST2 activity and increase in ERK activation. The decline in MST2 activity is due to Akt-mediated MST2 phosphorylation[17] (Figs 5d and 6d).

As Raf-1 and RASSF1A compete for MST2 binding[14], we examined the effects of RASSF1A (Fig. 1b). We downregulated endogenous RASSF1A in HeLa cells and transfected RASSF1A into MCF7, which lack endogenous RASSF1A expression. Changing RASSF1A abundance did not affect the kinetics of Akt activation by serum. In contrast, RASSF1A overexpression enhanced basal MST2 activity and delayed its downregulation. In addition, RASSF1A expression enhanced the amplitude and duration of MEK and ERK activation, whereas endogenous RASSF1A downregulation had the opposite effect. Furthermore, RASSF1A expression strongly reduced Raf-1 binding to MST2 while enhancing Raf-1 binding to MEK in both serum-starved and stimulated MCF7 (Fig. 1c). Downregulation of endogenous RASSF1A in HeLa cells had the opposite effects. These data demonstrate that the ERK and MST2 pathways crosstalk during growth factor stimulation, and that RASSF1A modulates this crosstalk.

These data also suggested that changes in Raf-1 binding to MEK or MST2 are critical for this crosstalk. We previously mapped the Raf-1-binding site in MST2 to a small segment of the MST2 SARAH domain[14]. A peptide, containing this sequence and stearylated to make it cell permeable, efficiently disrupted the MST2–Raf-1 interaction when added to cells (Fig. 1d) and *in vitro* (Supplementary Fig. 1a). A scrambled sequence control peptide was ineffective. The forced dissociation of MST2 from Raf-1 strongly increased MEK binding to Raf-1 and activated MEK and ERK (Fig. 1d). The disruptor peptide did not affect binding of Raf-1 to other known interaction partners, for example KSR1, HSP90 or 14-3-3 (Supplementary Fig. 1b). These results confirmed that changes in the MST2–Raf-1 interaction regulate the ERK pathway.

Therefore, we mapped the Raf-1 domains involved in MST2 binding using peptide arrays (Supplementary Fig. 1c). MST2 bound to Raf-1 through two distinct sites that overlap the Ras-binding domain (RBD) and partially the MEK-binding domain[7]. Thus, MST2 could interfere with Ras activation of Raf-1 and MEK phosphorylation, and RASSF1A may further influence these effects. We tested this hypothesis using the constitutively active HRasV12S35 mutant that selectively binds Raf kinases[20,21]. In MCF7 cells, binding of MST2 to Raf-1 was diminished by transfection of RASSF1A or HRasV12S35 and almost abolished by co-expression of both constructs. RASSF1A enhanced the HRasV12S35-Raf-1 interaction and the activation of ERK (Fig. 1e). Conversely, in HeLa cells, HRasV12S35 removed Raf-1 from MST2, whereas RASSF1A downregulation decreased Raf-1 binding to HRasV12S35 and the activation of ERK (Fig. 1f). These changes were due to MST2 competing for Raf-1 binding, as MST2 downregulation in HeLa cells augmented the interaction of Raf-1 with HRasV12S35 and ERK activation (Fig. 1g).

Conditions for switch-like transitions

These experiments demonstrated that dynamic protein interaction changes can coordinate signal distribution between the ERK and MST2 pathways. To analyse the conditions for such changes, we constructed a simple mathematical model, where proteins Y and Z compete for binding to X, and which considers only changes in protein concentrations (Fig. 2a and Supplementary Data). The concentrations of Raf-1, MST2 and MEK in cells are within a fourfold range (Supplementary Fig. 2a,b). Only if the affinities of Y and Z are very different, a rise in concentration of the high-affinity binder will decrease the binding of X to the low-affinity binder in a nonlinear fashion. Otherwise, the transitions between XY and XZ are smooth. This result agrees with *in vitro* experiments where a MST2–Raf-1 protein complex was incubated with increasing amounts of purified recombinant MEK protein that displaced MST2 from Raf-1 in a linear manner (Supplementary Fig. 2c). In cells, however, gradual changes in the concentrations of MEK and MST2 caused by dosed short interfering RNA (siRNA) transfections induced abrupt transitions between MST2–Raf-1 and MEK–Raf-1 complexes (Fig. 2b). These switch-like transitions cannot be explained by only varying the concentrations of the interaction partners.

Therefore, we extended the model by including that competing binding partners can exist in high- and low-affinity interaction states generated by changes in post-translational modifications (Fig. 2c and Supplementary Data). Here, the modified proteins (X_1 and Y_1) have reduced affinities for each other, but increased affinities for other binding partners (A and B). In this model steep state transitions occur when the modification reactions operate under saturating conditions. These results suggested that the switch-like transitions observed in cells involve post-translational modifications that change binding affinities; for example, MST2 and Raf-1 phosphorylation.

Feedback phosphorylation of Raf-1 by LATS1

We previously showed that Akt phosphorylation of MST2 enhances binding to Raf-1 (ref. 17). Therefore, we investigated whether Raf-1 phosphorylation also could modulate binding to MST2 (Fig. 3a). In resting cells, Raf-1 is phosphorylated on Ser 259, and the dephosphorylation of this residue is a prerequisite for Ser 338 phosphorylation and Raf-1 activation[22–24]. Serum stimulation induced Ser 259 dephosphorylation and phosphorylation of the activating Ser 338 site. Interestingly, RASSF1A expression (Fig. 3a) or the disruptor peptide (Fig. 1d) induced similar changes indicating that pS259 may be protected when Raf-1 interacts with MST2. Indeed, Raf-1 bound to MST2 seemed quantitatively phosphorylated on Ser 259, but lacked detectable Ser 338 phosphorylation. Mutating Ser 259 diminished Raf-1 binding to MST2 and activated both MST2 and ERK (Fig. 3b). Expression of RASSF1A augmented these effects. Performing this experiment in Raf-1 knockout mouse embryonic fibroblasts (MEFs) reconstituted with wild-type (WT) Raf-1 or Raf-1S259A confirmed that Ser 259 phosphorylation enhances MST2–Raf-1 interactions (Supplementary Fig. 3a). In contrast, mutating Ser 338 had no effect (Supplementary Fig. 3b). Thus, pS259 has a dual role in the crosstalk; it suppresses activation of the ERK pathway by preventing Raf-1 activation, and also suppresses activation of MST2 by promoting the inhibitory association with Raf-1.

Known Ser 259 kinases include PKA (refs 25,26) and Akt, whose role is disputed[7]. However, the kinase that maintains basal Ser 259 phosphorylation remains elusive. Interestingly, basal Raf-1 Ser 259 phosphorylation was decreased in *LATS1*$^{-/-}$ MEFs (Fig. 3c). This reduction could be reversed by reconstituting physiological LATS1 levels. Serum-induced dephosphorylation of Ser 259 and

© 2014 Macmillan Publishers Limited. All rights reserved.

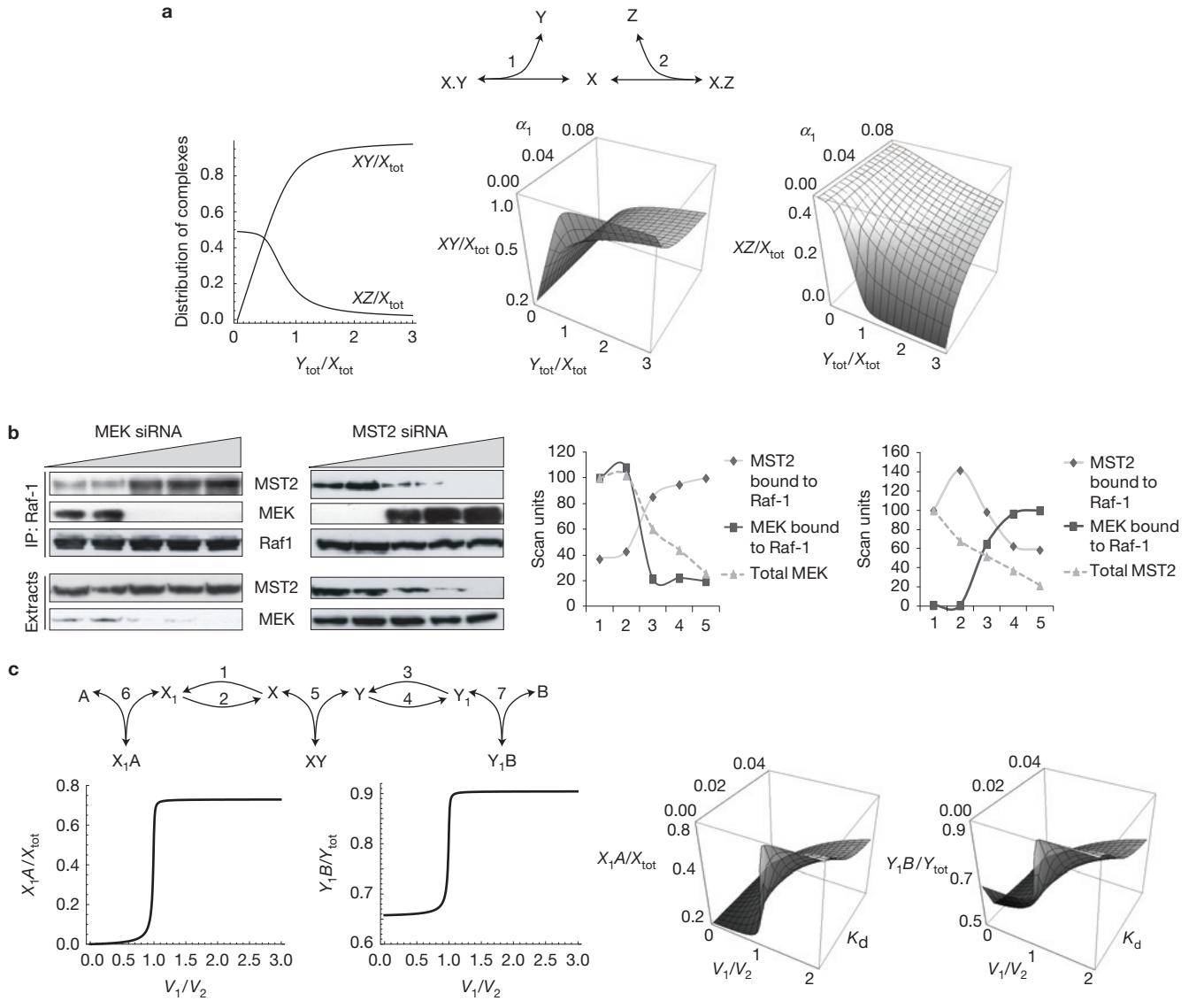

Figure 2 Competing protein interactions can cause switch-like transitions. (**a**) A simple mathematical model for the formation of two competing protein complexes (*XY* versus *XZ*). α_1 and α_2 are the dissociation constants of complexes *XY* and *XZ* normalized by X_{tot}. $\alpha_1 = 0.001$, $\alpha_2 = 0.01$, $Z_{tot}/X_{tot} = 0.5$. (**b**) HeLa cells were transfected with increasing amounts (0–10 ng) of MEK or MST2 siRNAs. Raf-1 immunoprecipitates were analysed for co-precipitating MEK and MST2. (**c**) Top left, a mathematical model considering that binding partners can exist in different affinity states. Bottom left panels, dependence of the steady-state levels of X_1 and Y_1 on the ratio of maximum rate constants V_1/V_2 of reactions 1 and 2. *V* denotes maximum reaction velocity. Right panels, dependence of the steady-state levels of X_1A and Y_1B on the ratio of maximum rate constants V_1/V_2 at varying saturation levels of the reactions 1–4. See Supplementary Information for parameter values. Uncropped images of blots are shown in Supplementary Fig. 6.

phosphorylation of Ser 338 occurred normally in *LATS1*$^{-/-}$ MEFs, but led to higher Raf-1 and MEK activation. In contrast, inhibition of Akt activation did not affect Ser 259 phosphorylation (Supplementary Fig. 3c). Furthermore, Raf-1 binding to MST2 was reduced in the *LATS1*$^{-/-}$ cells, but restored in the reconstituted MEFs. The levels of Ser 259 phosphorylation and Raf-1 bound to MST2 correlated closely under all conditions suggesting that Raf-1 associated with MST2 is quantitatively phosphorylated on Ser 259. Downregulation of LATS1 by increasing amounts of siRNA severely decreased Ser 259 phosphorylation inducing a switch-like change from MST2–Raf-1 to MEK–Raf-1 complexes and an activation of Raf-1, ERK and MST2 (Supplementary Fig. 3d). Therefore, we examined whether LATS1 is a Ser 259 kinase. LATS1 phosphorylated Ser 259 *in vitro*, whereas MST2 or kinase-dead LATS1 was ineffective (Fig. 3d). These data suggest that LATS1 is a genuine Ser 259 kinase that maintains basal levels of Ser 259 phosphorylation, thereby restraining both MST2 and ERK pathway activation.

A mathematical model for signal coordination

The above experiments demonstrate an important role for competing protein interactions in coordinating the activities of the Raf-1 and MST2 pathways. However, the combination of several competing protein interactions, the overlaid dynamic regulation by both Raf-1 and MST2 phosphorylations, and the resulting nonlinear behaviour

© 2014 Macmillan Publishers Limited. All rights reserved.

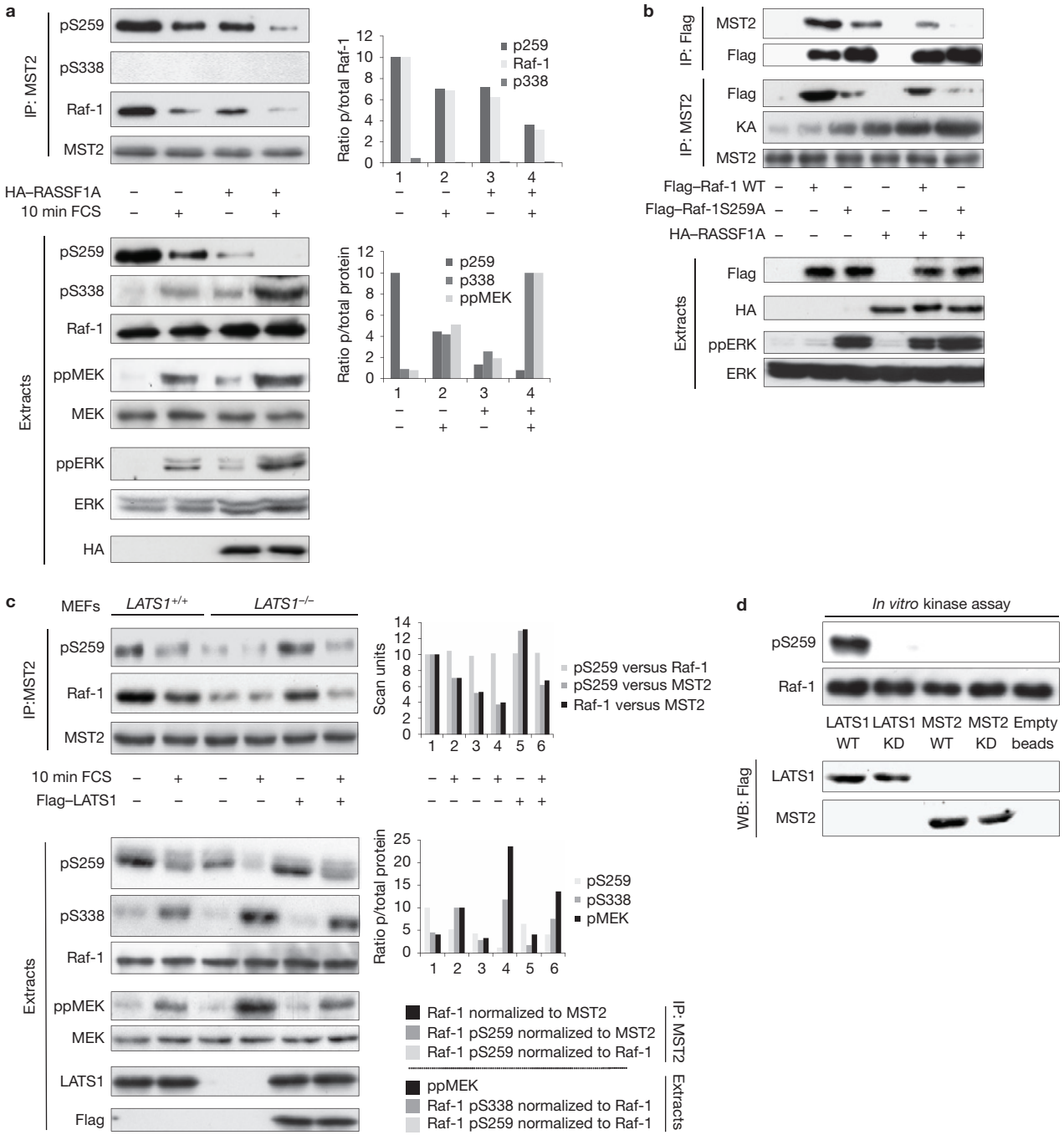

Figure 3 LATS1 phosphorylation of Raf-1 Ser 259 regulates MST2–Raf-1 complex formation. (**a**) Raf-1 phosphorylation and MST2 binding was assessed in MCF7 cells transfected with HA–RASSF1A or empty vector. (**b**) MCF7 cells were co-transfected with WT Flag–Raf-1 or Flag–Raf-1S259A and HA–RASSF1A as indicated. Raf-1 and MST2 binding, and MST2 kinase activity (KA), were analysed. (**c**) MST2 immunoprecipitates from *LATS1*$^{+/+}$, *LATS1*$^{-/-}$ and *LATS1*$^{-/-}$ MEFs reconstituted with Flag–LATS1 were analysed for Raf-1 co-precipitation and phosphorylation. (**d**) *In vitro* phosphorylation of recombinant Raf-1 by WT or kinase-dead (KD) Flag-tagged LATS1 and MST2. Uncropped images of blots are shown in Supplementary Fig. 6.

hamper an intuitive analysis. To systematically explore the emergent properties of this circuitry, we developed a mathematical model that incorporated protein interactions, phosphorylation reactions and feedback loops using Michaelis–Menten descriptions of reactions at steady state. To ascertain that protein interactions dynamics are properly captured, we also developed a mass-action law model where enzyme reactions are described at the elementary step level. Both models gave fully consistent results (Section 3 of Supplementary Note). Complete model descriptions are presented in the Supplementary Note.

Briefly, the reaction scheme (Fig. 4a) encompasses growth factor receptors that activate Ras and Raf-1, and PI(3)K and its effector Akt. The PI3K–Akt axis can also be activated by Ras. Thus, active Ras and Akt were taken as inputs to the model. When exploring the effects of

© 2014 Macmillan Publishers Limited. All rights reserved.

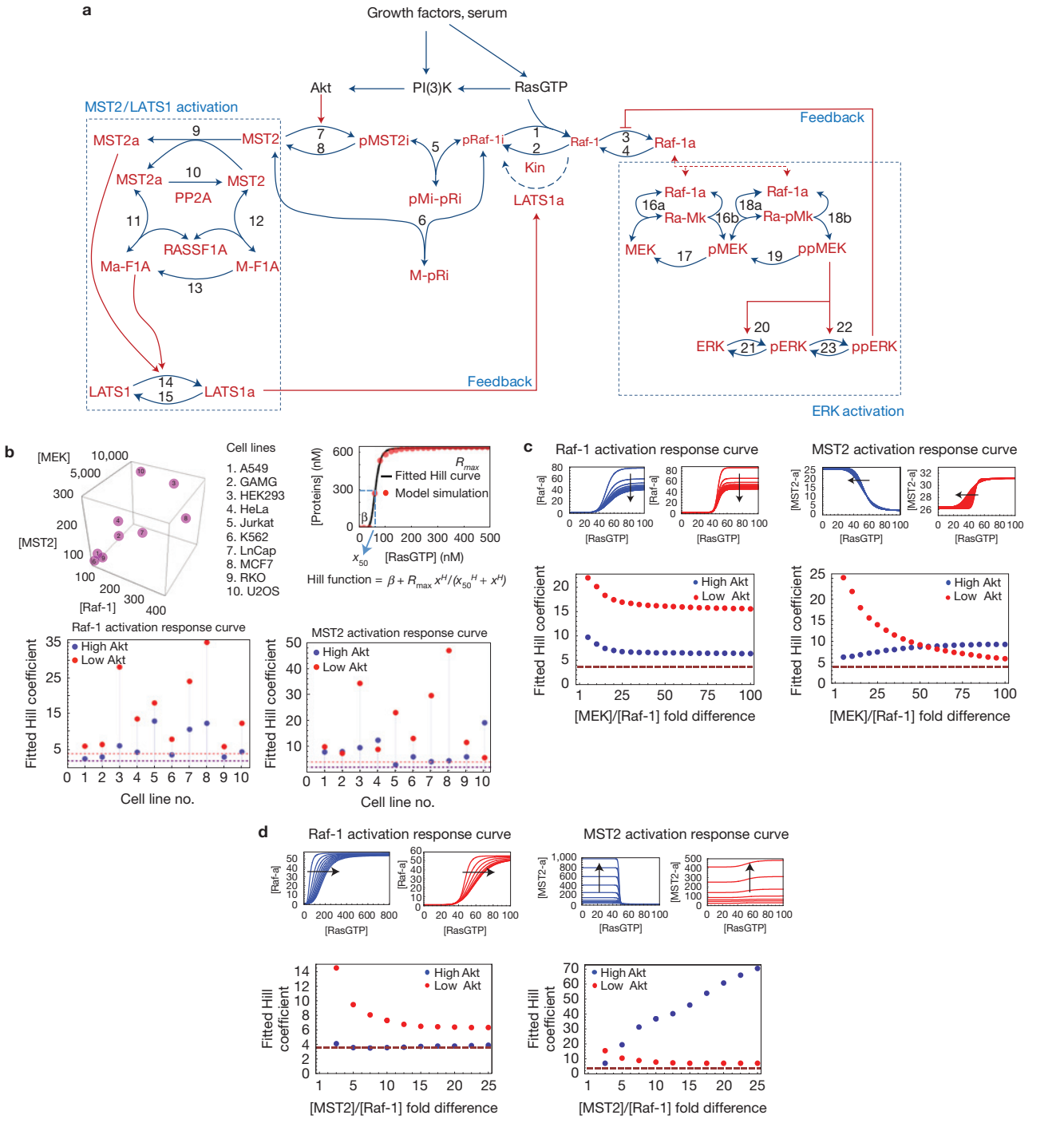

Figure 4 A mathematical model for MST2 and ERK pathway crosstalk. (**a**) Kinetic scheme showing the molecular species considered as inputs to the system in black, and the reactant proteins involved in binding and (de)phosphorylation reactions in red: Raf-1a, active Raf-1 phosphorylated at Ser 338; pRaf-1i, inactive Raf-1 phosphorylated at Ser 259; pMST2i, inactive MST2 phosphorylated by Akt; MST2a, activated MST2; pMi-pRi, pMST2i–pRaf-1i complex; M-pRi, MST2–pRaf-1i complex; M-F1A, RASSF1A–MST2 complex; Ma-F1A, MST2a–RASSF1A complex; LATS1a, active LATS1; pMEK, pERK, single-phosphorylated, low-activity MEK or ERK; ppMEK, ppERK, double-phosphorylated, high-activity MEK or ERK; Ra-Mk, Ra-pMk, complexes of Raf-1a and MEK and pMEK; Kin, kinases other than LATS1 phosphorylating Raf-1 on Ser 259 indicated by a broken line. (**b**) Three-dimensional plot showing the concentrations of Raf-1, MST2 and MEK1/2 in 10 cell lines[51]. Hill coefficients (*H*) of Raf-1 and MST2 activation in response to increasing Ras activation (RasGTP) were derived: β = offset, R_{max} = maximal response, ×50 = half-maximal threshold. As Akt activity can influence the switching behaviour, Hill coefficients were calculated under low (red dots) and high (blue dots) Akt activities. Hill coefficients of >2 indicate switch-like behaviour, and Hill coefficients >4 strong switches. (**c**) [MEK]/[Raf-1] concentrations were varied 1–100-fold versus fixed [Raf-1] = 100 nM. The arrows in the upper panels indicate respective changes of the dose–response curves in the direction of increasing [MEK]/[Raf-1] fold differences. Hill coefficients for the Raf-1 and MST2 activation curves in response to increasing RasGTP level under high or low Akt activities were calculated. (**d**) The same as in **c** except that the [MST2] concentration was varied 1–100-fold. In all cases, Hill coefficients are ≥4, indicating strong switches over the whole concentration range of MEK or MST2.

© 2014 Macmillan Publishers Limited. All rights reserved.

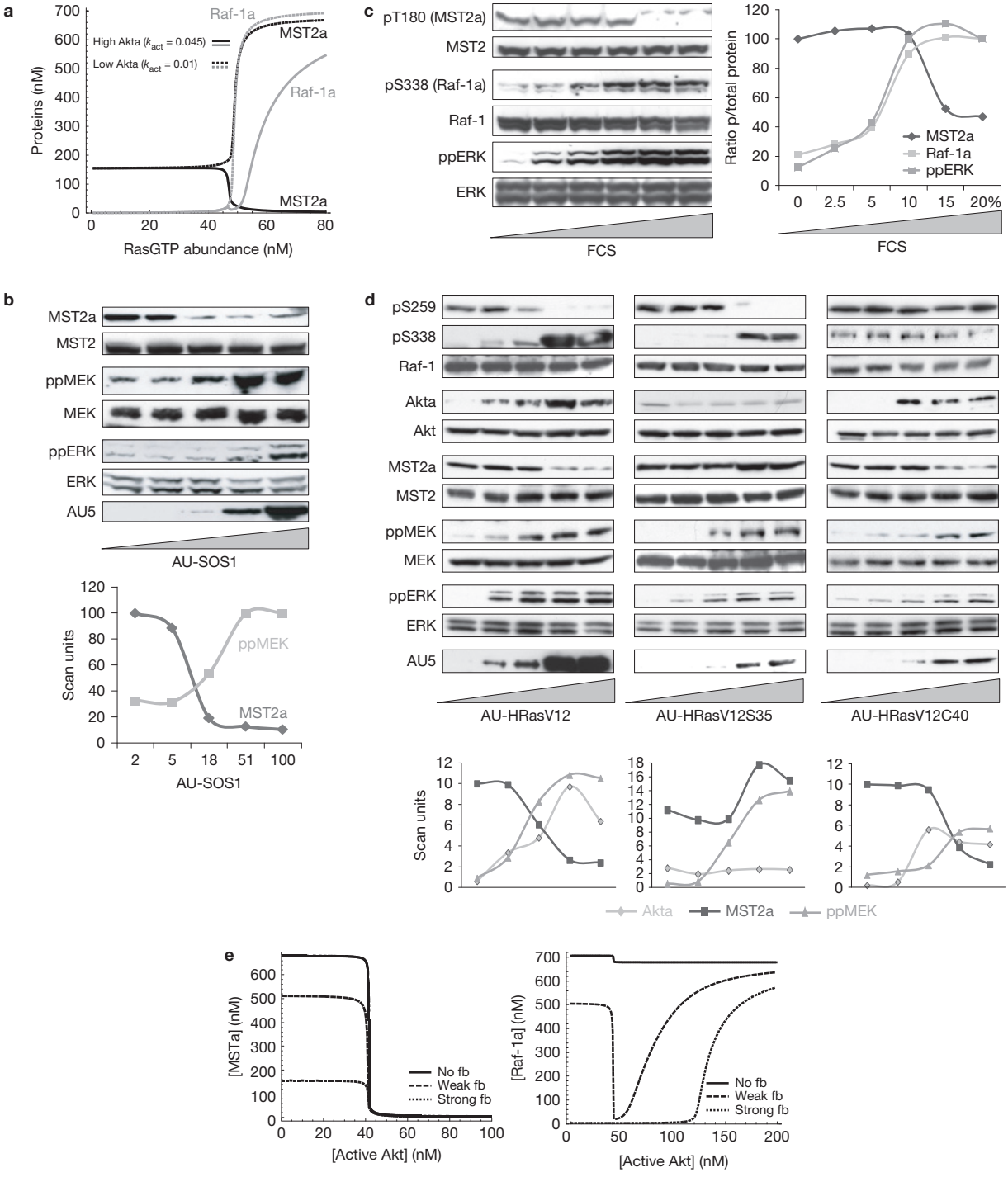

Figure 5 Model analysis and experimental validation. (**a**) Switch-like dependence of Raf-1 (Raf-1a) and MST2 (MST2a) activation on RasGTP and Akt activity. (**b**) HeLa cells transfected with 0–1.5 μg of AU5-tagged-SOS1 plasmid were analysed for MST, MEK and ERK activation. (**c**) Extracts of serum-starved HeLa cells treated with 0–20% FCS (5 min) were assayed for activating MST2, Raf-1 and ERK phosphorylations. (**d**) HeLa cells were transfected with plasmids (0–1 μg) encoding AU5-tagged HRasV12, HRasV12S35 and HRasV12C40 (right panel). Raf-1 phosphorylation and activation of Akt, MST2, MEK and ERK were assessed. (**e**) Akt regulation of Raf-1 and MST2 at strong Ras activation ([RasGTP] = 50 nM) and different activities of the LATS1 feedback loop (fb; k2a = {0, 0.01, 0.02}). Uncropped images of blots are shown in Supplementary Fig. 6.

Ras, Akt activity was modelled as a function of active Ras, whereas for simulations of serum effects both Ras and Akt activities were considered functions of serum. Active Ras disrupts the MST2–Raf-1 complex activating Raf-1 and the ERK pathway. Raf-1 activation is complex, but the dephosphorylation of Ser 259 and the subsequent phosphorylation of Ser 338 are essential[7,8,23]. These phosphorylations are mutually exclusive[27] and were modelled as separate events. Raf-1 phosphorylated on Ser 259 (pRaf-1i) binds and inhibits

© 2014 Macmillan Publishers Limited. All rights reserved.

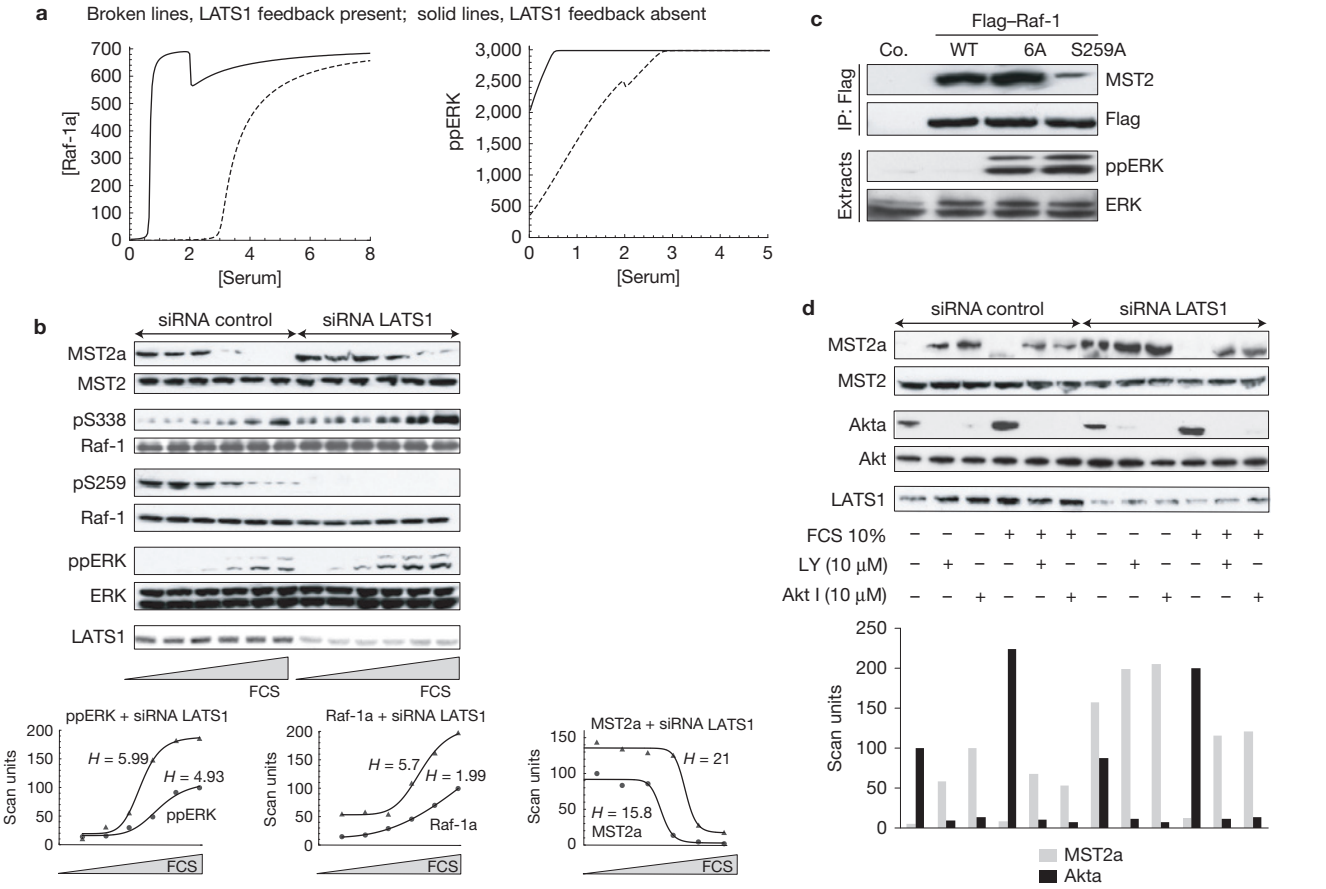

Figure 6 The LATS1 feedback loop regulates ERK pathway activation. (**a**) Simulation of serum-stimulated Raf-1 and ERK activation in the absence ($k_{2a}=0.003$) or presence ($k_{2a}=0.01$) of the LATS1 feedback loop. [RasGTP] = 5 nM, $k_{sr1}=1$, $k_{act}=0.01$, $k_1=0.05$. (**b**) HeLa cells were transfected with control or LATS1 siRNA. Serum-starved cells were stimulated with 0–20% FCS (5 min). Extracts were analysed by western blotting. Hill coefficients (H) were calculated from curves fitted to quantified phospho-protein levels normalized by respective total protein levels. (**c**) HeLa cells were transfected with Flag-tagged Raf-1 constructs corresponding to WT, S259A or 6A (all six ERK feedback phosphorylation sites mutated to alanine)[30]. Flag immunoprecipitates from serum-starved cells were examined for associated MST2. Co., immunoprecipitate with species-matched control IgG. (**d**) HeLa cells were transfected as in **b**, treated with the PI(3)K inhibitor LY294002 (LY) or Akt inhibitor (Akt I) for 30 min, and then with 10% FCS for 5 min. Extracts were analysed by western blotting. Uncropped images of blots are shown in Supplementary Fig. 6.

MST2, whereas Raf-1 phosphorylated on Ser 338 (Raf-1a) binds and activates MEK. The ERK pathway model includes the double (de)phosphorylation cycles of MEK and ERK (refs 28,29) and the negative feedback from ERK to Raf-1 (refs 29,30). Active Akt phosphorylates and inhibits MST2 yielding inactive pMST2i that binds to pRaf-1i (ref. 17). Active MST2 (MST2a) is generated by dimerization and autophosphorylation in *trans*[10,31,32]. MST2 activation is enhanced by binding to RASSF1A (refs 14,17,33,34), and RASSF1A protects activating MST2 phosphorylations from phosphatases[35]. Thus, we assumed that RASSF1A is associated preferentially with MST2a, and that MST2 can be activated while bound to RASSF1A. These assumptions are consistent with present knowledge and resulted in simulations that most closely reproduced experimental findings. MST2a phosphorylates and activates LATS1 (refs 14,33,36), which in turn phosphorylates Raf-1 on Ser 259, blocking the ability of Raf-1 to activate the ERK pathway and promoting Raf-1 binding to MST2.

Model analysis revealed non-intuitive dynamic properties of the MST2–Raf-1 interaction. The most remarkable was the occurrence of sharp switches, which appear when the Raf-1 (de)phosphorylation (reactions 1–4) and the MST2 (de)phosphorylation (reactions 7–8) cycles are saturated; that is, when the concentrations of Raf-1 and MST2 are larger than the Michaelis–Menten constants (K_m) of the respective reactions. Switching is most abrupt if the (de)phosphorylation cycles of both proteins are saturated, less abrupt if only one cycle is saturated, and almost disappears if neither cycle is saturated. Determining the concentrations of Raf-1, MST2 and MEK by quantitative western blotting in MCF7 and HeLa cells showed that the conditions for sharp switches are satisfied (Supplementary Fig. 2a,b and Tables 3 and 6). A survey of 10 cell lines revealed that conditions for switches are common (Fig. 4b). In addition, altering the ratios of MEK or MST2, respectively, versus Raf-1 between 1- and 100-fold resulted in switches over the whole concentration range showing that switches are a robust property of this network (Fig. 4c,d).

Another important model prediction was that increasing Ras activity should cause sharp off–on switches in MST2 and Raf-1 activities (Fig. 5a). MST2 switches on at low and off at high Akt activity, but Raf-1 switches on under either condition. To test this prediction we expressed increasing amounts of AU5-tagged SOS1

© 2014 Macmillan Publishers Limited. All rights reserved.

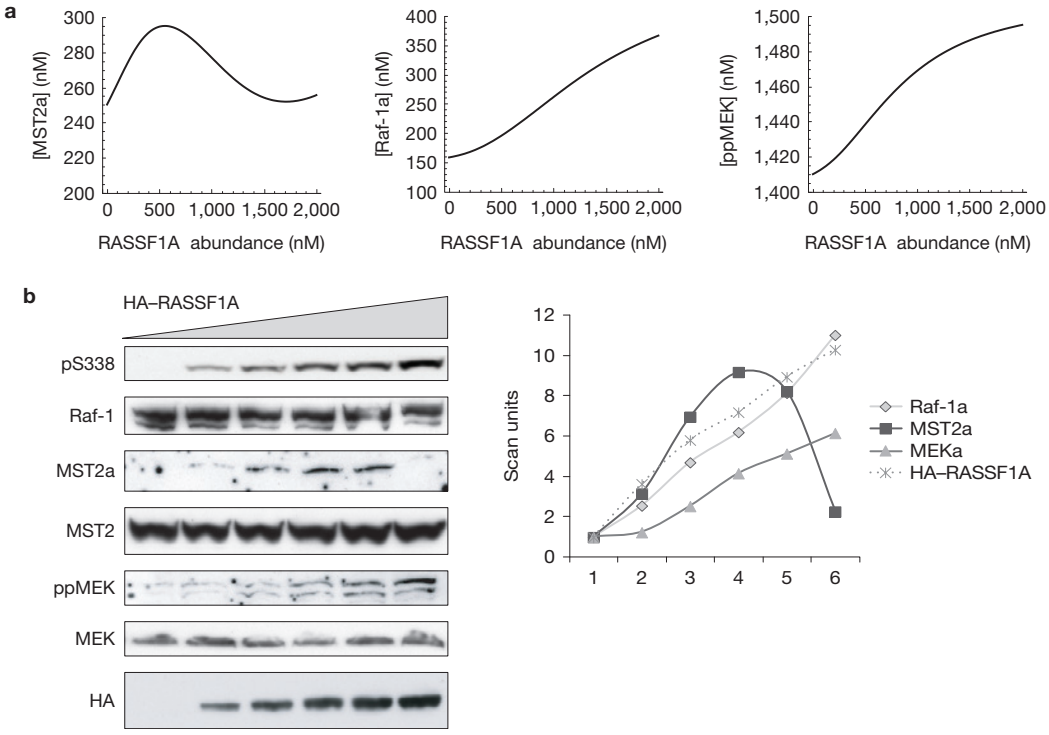

Figure 7 RASSF1A regulation of MST2 and ERK activation. (**a**) Simulated effects of increasing RASSF1A levels on the levels of active Raf-1, MST2 and MEK. Parameters used are $K_{m1} = K_{m2a} = K_{m2b} = K_{m3} = K_{m4} = K_{m7} = K_{m8} = 50$, $k_{act} = 0.01$. (**b**) MCF7 cells transfected with 0–1 μg of HA-tagged RASSF1A were analysed for Raf-1, MEK and ERK activation. The graphs show quantification of RASSF1A and the phospho-proteins normalized to corresponding total protein levels. Uncropped images of blots are shown in Supplementary Fig. 6.

guanine nucleotide exchange factor, which activates endogenous Ras. Increasing AU5–SOS1 expression switched on Raf-1 but switched off MST2 activities (Fig. 5b). The same behaviour occurred when cells were stimulated with increasing amounts of serum (Fig. 5c). To dissect the role of Akt we transfected cells with increasing amounts of H-RasV12 or the Ser 35 (S35) and Cys 40 (C40) effector domain mutants, which selectively activate Raf-1 or PI(3)K, respectively (Fig. 5d). Similarly to serum stimulation or SOS1 transfection, H-RasV12 activated ERK and Akt, while switching off MST2. H-RasV12S35 switched on both ERK and MST2, whereas H-RasV12C40 activated Akt and switched off MST2. Consistent with the experimental data, increasing Akt activity in the model precipitously inhibited MST2, whereas Raf-1 activity was affected only when the LATS1 feedback of inhibitory Ser 259 phosphorylation was operating (Fig. 5e). Thus, Ras can activate both ERK and MST2 pathways, but owing to the Akt-mediated MST2 inhibition Ras switches off MST2 in cells where Ras activates Akt strongly.

The LATS1 feedback phosphorylation of Raf-1 affected both MST2 and ERK pathways. As expected this feedback reduced MST2 activity (Fig. 5e), but interestingly, modelling indicated that it also renders Raf-1 and ERK less sensitive to activation (Fig. 6a). Reducing the feedback by LATS1 downregulation made Raf-1 and ERK activation by serum stronger and more switch-like, in particular Raf-1 activation (Fig. 6b). Switching was less pronounced at the level of ERK presumably owing to the already switch-like activation kinetics caused by multi-site phosphorylation[28,37]. In contrast, the negative feedback from ERK to Raf-1 (refs 29,30) did not affect Raf-1 regulation of MST2, as mutation of the ERK feedback phosphorylation sites in Raf-1 did not change MST2 binding (Fig. 6c). Serum still switched off MST2, although higher concentrations were required when LATS1 was downregulated. The eventual inhibition of MST2 is due to Akt, which can deactivate MST2 (ref. 17) in a manner independent of the LATS1 feedback (Fig. 6d).

Another unexpected finding from the model analysis was that increasing RASSF1A levels generate a linear increase in Raf-1 and MEK activities, but a nonlinear activation of MST2 (Fig. 7a). To test these predictions experimentally, we gradually increased RASSF1A expression in MCF7 cells (Fig. 7b) observing a dose-dependent linear increase of Raf-1 and MEK activities, but a bell-shaped MST2 activation curve. These experiments support a dual function of RASSF1A as a nonlinear regulator of the MST2 pathway and as a linear amplifier of ERK signalling.

Switches regulate biological outcomes

To determine the biological effects of signalling switches we used the Raf-1S259A mutant, which constitutively stimulates ERK signalling[38], but has reduced control over MST2. Expression of Raf-1S259A, but not WT Raf-1, accelerated cell proliferation, which was significantly enhanced when MST2 was downregulated (Fig. 8a). Testing whether this impairment was due to apoptosis induction we found that Raf-1S259A, but not WT Raf-1, augmented apoptosis, which was completely blocked by MST2 downregulation (Fig. 8b). Conversely, Raf-1S259A efficiently stimulated long-term survival and proliferation in colony-forming assays when MST2 was depleted (Fig. 8c). For

© 2014 Macmillan Publishers Limited. All rights reserved.

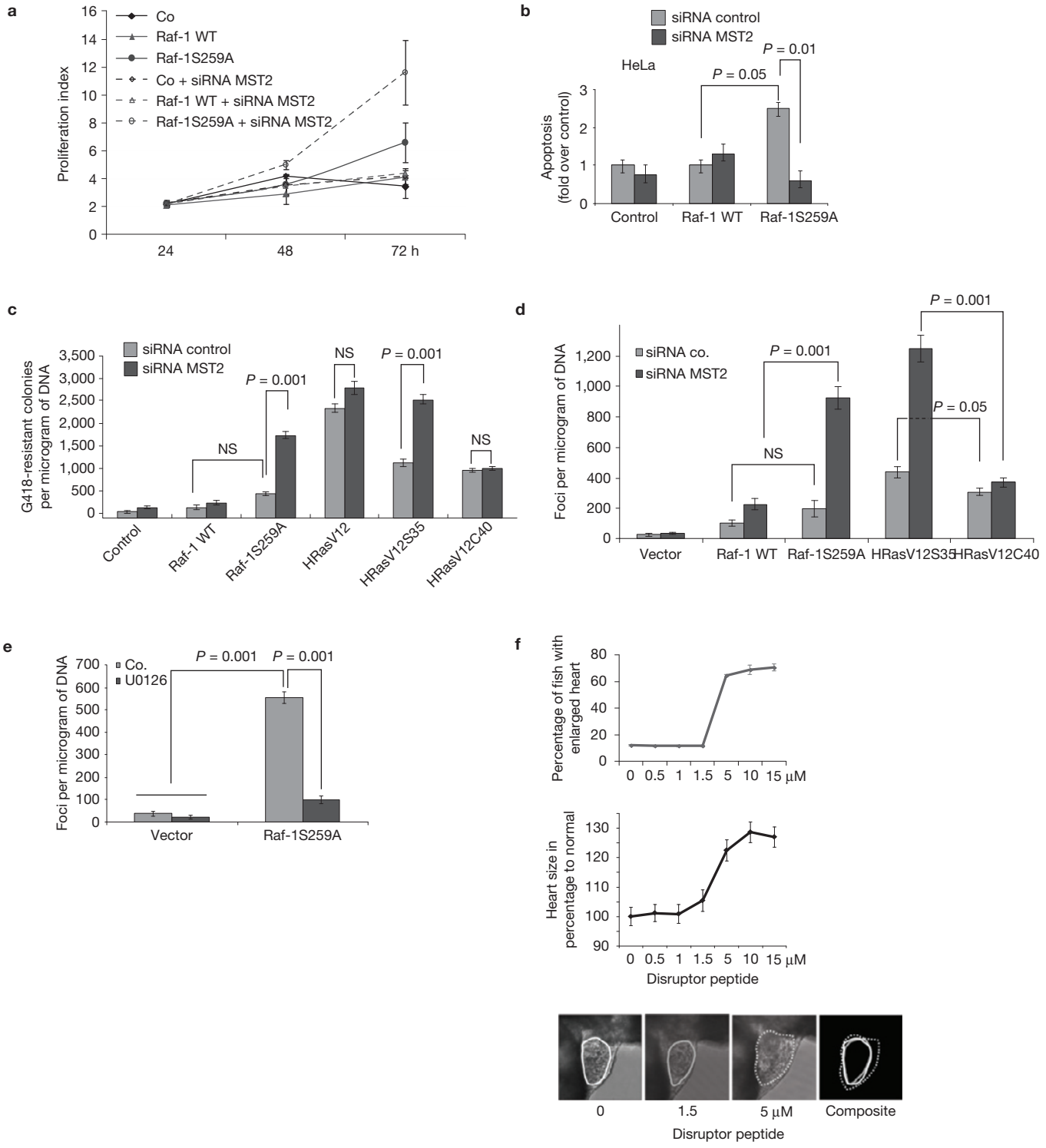

Figure 8 MST2 and ERK pathway crosstalk regulates cell proliferation, survival and transformation. (**a**) HeLa cells were co-transfected as indicated. Co, empty vector. Proliferation was assayed by flow cytometry ($n = 3$). Error bars for all panels = s.e.m.; n, number of independent experiments. (**b**) HeLa cells were co-transfected as indicated. Apoptosis was assayed by quantifying DNA fragmentation by flow cytometry ($n = 5$). P values for **b**–**e** were calculated using Student's t-test. (**c**) NIH3T3 cells were co-transfected with indicated expression vectors, a G418 resistance marker, and either control or MST2-specific siRNAs. Cells were selected with G418 for 12 days and surviving colonies were counted ($n = 6$). (**d**) NIH3T3 cells were co-transfected as in **c** and grown to confluence. Transformed foci per microgram of transfected DNA were scored two weeks later ($n = 6$). (**e**) NIH3T3 focus assays were carried out as in **d** ±5 µM U0126 ($n = 6$). (**f**) Zebrafish embryos were treated with increasing doses of disruptor peptide. Heart size (outlined in white and grey lines) was measured at day 3 using 15 embryos per condition. Plots show the percentage of embryos with enlarged hearts and change in heart size. Error bars represent s.e.m. ($n = 3$).

© 2014 Macmillan Publishers Limited. All rights reserved.

reference, RasV12-stimulated colony growth was not significantly changed by downregulating MST2. In contrast, the number of colonies induced by H-RasV12S35 (which selectively binds Raf-1) was intermediate, but MST2 depletion increased it to the level induced by RasV12. MST2 knockdown had no effect on colony formation induced by RasV12C40 (which selectively binds PI(3)K). These findings indicate that the concomitant activation of MST2 by Ras counteracts cell survival and proliferation stimulated by Raf-1, and that PI(3)K activation neutralizes the MST2 effects.

We also examined cell transformation using focus formation assays (Fig. 8d). Interestingly, Raf-1S259A transformed cells when MST2 was downregulated. MST2 downregulation also enhanced the transforming potential of RasV12S35, but not of RasV12C40. Raf-1S259A-induced transformation was sensitive to MEK inhibition (Fig. 8e), demonstrating its dependence on the ERK pathway. Interestingly, transformation by Raf-1S259A was also enabled by expression of a constitutively active PI(3)K mutant, which had little transforming ability on its own (Supplementary Fig. 4). These findings suggest that in respect to cell transformation, MST2 downregulation is functionally equivalent to PI(3)K activation.

Finally, we examined whether these biochemical network switches could induce phenotypic switches at the level of an organism (Fig. 8f). Yap activity is important for heart development in zebrafish[39]. Treating zebrafish embryos with the cell-permeable disruptor peptide increased heart size. A dose response curve showed that this phenotype transition occurred in a switch-like fashion.

DISCUSSION

Switch-like kinetics play important roles in signal transduction mechanisms that govern cell fate decisions. They can be caused by different mechanisms including multisite phosphorylation, zero-order ultrasensitivity, positive or double-negative feedback loops, and substrate competition[40–44]. A classic example is the dual phosphorylation of MAPKs, which conveys ultrasensitivity that triggers *Xenopus* oocyte maturation[37]. This analysis suggested that network dynamics can encode biological decision making. Our discovery that a combination of competing protein interactions and phosphorylation-mediated affinity changes generates sharp switches adds an important mechanism to the regulation of signal transduction networks that rely on protein interactions for information processing (Supplementary Fig. 5). Importantly, the conditions for such switches are commonly satisfied in cell lines (Fig. 4b), and also can induce phenotypic switches at the organ level (Fig. 8f).

Our mathematical model allowed us to identify and experimentally test the critical elements that govern linear versus switching behaviour in the MST2—Raf-1 network, revealing three interconnected layers of regulation. One pertains to the relative concentrations and affinities of the proteins involved in the competing interactions. Increasing the concentration of one interaction partner causes a linear increase in protein complex formation at the expense of the competing protein complex. Steep transitions are observed only in the low-affinity protein complex, when the affinity of the competing binder is substantially higher. The second and most influential layer is the regulation of Raf-1 and MST2 by phosphorylation that changes the binding affinities. These reactions confer switch-like behaviour, if they are operating under saturating conditions. The criteria conferring switch-like behaviour are satisfied across different cell types and concentration ranges (Fig. 4b–d), indicating that this mechanism may be widely used to make cell fate decisions and shape organs. The third layer of regulation is the LATS1-mediated feedback phosphorylation of Raf-1 on Ser 259, which negatively regulates the activities of both pathways. Raf-1 phosphorylated on Ser 259 is inactive towards the ERK pathway, and its dephosphorylation is part of the physiological Raf-1 activation process[23]. On the other hand, Ser 259 phosphorylation promotes Raf-1 binding to MST2 and MST2 inhibition. Thus, mitogen-induced Ser 259 dephosphorylation will activate both proliferation and apoptosis. An intrinsic coupling between proliferation and apoptosis seems sensible for multi-cellular organisms where the unlicensed proliferation of a single cell poses a much greater risk for the organism than the demise of this cell. This property was first discovered in the c-Myc transcription factor[45,46], but recent evidence suggests that such integration also occurs in cytosolic signal processing[47].

Previous work showed that the Raf-1S259A mutant could stimulate ERK pathway activation and cell proliferation, but failed to support cell transformation[38]. Our present results suggest that this paradox is due to the loss of negative control over the MST2 pathway caused by this mutation. Interestingly, Ser 259 phosphorylation is reduced in Raf-1 mutants found in Noonan and related syndromes[48–50], which are genetic disorders characterized by mental retardation, cardiac defects, and abnormalities in skin pigmentation and facial structures. These Raf-1 mutations are strongly associated with hypertrophic cardiomyopathy[48–50]. This is remarkably similar to the phenotype we observed in zebrafish on disruption of the MST2–Raf-1 interaction (Fig. 8f), emphasizing the role of Ser 259 phosphorylation in pathophysiological signalling. The discovery that LATS1 is a Ser 259 kinase adds another aspect to efforts aiming to elucidate the mechanistic basis of these genetic syndromes. □

METHODS

Methods and any associated references are available in the online version of the paper.

Note: Supplementary Information is available in the online version of the paper

ACKNOWLEDGEMENTS

This work was supported by Science Foundation Ireland grant No. 06/CE/B1129 and the EU FP7 Projects PRIMES No. 278568 and ASSET No. 259348-2. We thank A. Blanco (Conway Core Technologies), T. Santra, J. Munoz and M. Dobrzynski for help with flow cytometry and modelling.

AUTHOR CONTRIBUTIONS

D.R., D.M., C.D. and M.H. performed the experiments, L.K.N. and B.N.K. performed the modelling, W.K. directed the overall research and all authors wrote the manuscript.

COMPETING FINANCIAL INTERESTS

The authors declare no competing financial interests.

Published online at www.nature.com/doifinder/10.1038/ncb2986
Reprints and permissions information is available online at www.nature.com/reprints

1. Kholodenko, B. N., Hancock, J. F. & Kolch, W. Signalling ballet in space and time. *Nat. Rev. Mol. Cell Biol.* **11,** 414–426 (2010).
2. Jorgensen, C. & Linding, R. Simplistic pathways or complex networks? *Curr. Opin. Genet. Dev.* **20,** 15–22 (2010).
3. Marshall, C. J. Specificity of receptor tyrosine kinase signaling: transient versus sustained extracellular signal-regulated kinase activation. *Cell* **80,** 179–185 (1995).

© 2014 Macmillan Publishers Limited. All rights reserved.

4. Murphy, L. O., Smith, S., Chen, R. H., Fingar, D. C. & Blenis, J. Molecular interpretation of ERK signal duration by immediate early gene products. *Nat. Cell Biol.* **4,** 556–564 (2002).
5. Nakakuki, T. *et al.* Ligand-specific c-Fos expression emerges from the spatiotemporal control of ErbB network dynamics. *Cell* **141,** 884–896 (2010).
6. Von Kriegsheim, A. *et al.* Cell fate decisions are specified by the dynamic ERK interactome. *Nat. Cell Biol.* **11,** 1458–1464 (2009).
7. Matallanas, D. *et al.* Raf family kinases: old dogs have learned new tricks. *Genes Cancer* **2,** 232–260 (2011).
8. Osborne, J. K., Zaganjor, E. & Cobb, M. H. Signal control through Raf: in sickness and in health. *Cell Res.* **22,** 14–22 (2012).
9. Chen, J., Fujii, K., Zhang, L., Roberts, T. & Fu, H. Raf-1 promotes cell survival by antagonizing apoptosis signal-regulating kinase 1 through a MEK–ERK independent mechanism. *Proc. Natl Acad. Sci. USA* **98,** 7783–7788 (2001).
10. O'Neill, E., Rushworth, L., Baccarini, M. & Kolch, W. Role of the kinase MST2 in suppression of apoptosis by the proto-oncogene product Raf-1. *Science* **306,** 2267–2270 (2004).
11. Ehrenreiter, K. *et al.* Raf-1 regulates Rho signaling and cell migration. *J. Cell Biol.* **168,** 955–964 (2005).
12. Avruch, J. *et al.* Protein kinases of the Hippo pathway: regulation and substrates. *Semin. Cell Dev. Biol.* **23,** 770–784 (2012).
13. Visser, S. & Yang, X. LATS tumor suppressor: a new governor of cellular homeostasis. *Cell Cycle* **9,** 3892–3903 (2010).
14. Matallanas, D. *et al.* RASSF1A elicits apoptosis through an MST2 pathway directing proapoptotic transcription by the p73 tumor suppressor protein. *Mol. Cell* **27,** 962–975 (2007).
15. Richter, A. M., Pfeifer, G. P. & Dammann, R. H. The RASSF proteins in cancer; from epigenetic silencing to functional characterization. *Biochim. Biophys. Acta* **1796,** 114–128 (2009).
16. Avruch, J. *et al.* Rassf family of tumor suppressor polypeptides. *J. Biol. Chem.* **284,** 11001–11005 (2009).
17. Romano, D. *et al.* Proapoptotic kinase MST2 coordinates signaling crosstalk between RASSF1A, Raf-1, and Akt. *Cancer Res.* **70,** 1195–1203 (2010).
18. Halder, G. & Johnson, R. L. Hippo signaling: growth control and beyond. *Development* **138,** 9–22 (2011).
19. Bossuyt, W. *et al.* An evolutionary shift in the regulation of the Hippo pathway between mice and flies. *Oncogene* **33,** 1218–1228 (2014).
20. White, M. A. *et al.* Multiple Ras functions can contribute to mammalian cell transformation. *Cell* **80,** 533–541 (1995).
21. Rodriguez-Viciana, P. *et al.* Role of phosphoinositide 3-OH kinase in cell transformation and control of the actin cytoskeleton by Ras. *Cell* **89,** 457–467 (1997).
22. Kubicek, M. *et al.* Dephosphorylation of Ser-259 regulates Raf-1 membrane association. *J. Biol. Chem.* **277,** 7913–7919 (2002).
23. Dhillon, A. S., Meikle, S., Yazici, Z., Eulitz, M. & Kolch, W. Regulation of Raf-1 activation and signalling by dephosphorylation. *EMBO J.* **21,** 64–71 (2002).
24. Jaumot, M. & Hancock, J. F. Protein phosphatases 1 and 2A promote Raf-1 activation by regulating 14-3-3 interactions. *Oncogene* **20,** 3949–3958 (2001).
25. Dhillon, A. S. *et al.* Cyclic AMP-dependent kinase regulates Raf-1 kinase mainly by phosphorylation of serine 259. *Mol. Cell. Biol.* **22,** 3237–3246 (2002).
26. Dumaz, N. & Marais, R. Protein kinase A blocks Raf-1 activity by stimulating 14-3-3 binding and blocking Raf-1 interaction with Ras. *J. Biol. Chem.* **278,** 29819–29823 (2003).
27. Dhillon, A. S., von Kriegsheim, A., Grindlay, J. & Kolch, W. Phosphatase and feedback regulation of Raf-1 signaling. *Cell Cycle* **6,** 3–7 (2007).
28. Markevich, N. I., Hoek, J. B. & Kholodenko, B. N. Signaling switches and bistability arising from multisite phosphorylation in protein kinase cascades. *J. Cell Biol.* **164,** 353–359 (2004).
29. Sturm, O. E. *et al.* The mammalian MAPK/ERK pathway exhibits properties of a negative feedback amplifier. *Sci. Signal.* **3,** ra90 (2010).
30. Dougherty, M. K. *et al.* Regulation of Raf-1 by direct feedback phosphorylation. *Mol. Cell* **17,** 215–224 (2005).
31. Anand, R., Kim, A. Y., Brent, M. & Marmorstein, R. Biochemical analysis of MST1 kinase: elucidation of a C-terminal regulatory region. *Biochemistry* **47,** 6719–6726 (2008).
32. Glantschnig, H., Rodan, G. A. & Reszka, A. A. Mapping of MST1 kinase sites of phosphorylation. Activation and autophosphorylation. *J. Biol. Chem.* **277,** 42987–42996 (2002).
33. Hamilton, G., Yee, K. S., Scrace, S. & O'Neill, E. ATM regulates a RASSF1A-dependent DNA damage response. *Curr. Biol.* **19,** 2020–2025 (2009).
34. Praskova, M., Khoklatchev, A., Ortiz-Vega, S. & Avruch, J. Regulation of the MST1 kinase by autophosphorylation, by the growth inhibitory proteins, RASSF1 and NORE1, and by Ras. *Biochem. J.* **381,** 453–462 (2004).
35. Guo, C., Zhang, X. & Pfeifer, G. P. The tumor suppressor RASSF1A prevents dephosphorylation of the mammalian STE20-like kinases MST1 and MST2. *J. Biol. Chem.* **286,** 6253–6261 (2011).
36. Chan, E. H. *et al.* The Ste20-like kinase Mst2 activates the human large tumor suppressor kinase Lats1. *Oncogene* **24,** 2076–2086 (2005).
37. Ferrell, J. E. Jr & Machleder, E. M. The biochemical basis of an all-or-none cell fate switch in Xenopus oocytes. *Science* **280,** 895–898 (1998).
38. Dhillon, A. S. *et al.* A Raf-1 mutant that dissociates MEK/extracellular signal-regulated kinase activation from malignant transformation and differentiation but not proliferation. *Mol. Cell. Biol.* **23,** 1983–1993 (2003).
39. Miesfeld, J. B. & Link, B. A. Establishment of transgenic lines to monitor and manipulate Yap/Taz-Tead activity in zebrafish reveals both evolutionarily conserved and divergent functions of the Hippo pathway. *Mech. Dev.* http://dx.doi.org/10.1016/j.mod.2014.02.003 (2014).
40. Sha, W. *et al.* Hysteresis drives cell-cycle transitions in Xenopus laevis egg extracts. *Proc. Natl Acad. Sci. USA* **100,** 975–980 (2003).
41. Qiao, L., Nachbar, R. B., Kevrekidis, I. G. & Shvartsman, S. Y. Bistability and oscillations in the Huang–Ferrell model of MAPK signaling. *PLoS Comput. Biol.* **3,** 1819–1826 (2007).
42. Kim, S. Y. & Ferrell, J. E. Jr Substrate competition as a source of ultrasensitivity in the inactivation of Wee1. *Cell* **128,** 1133–1145 (2007).
43. Kholodenko, B. N. Cell-signalling dynamics in time and space. *Nat. Rev. Mol. Cell Biol.* **7,** 165–176 (2006).
44. Salazar, C. & Hofer, T. Competition effects shape the response sensitivity and kinetics of phosphorylation cycles in cell signaling. *Ann. NY Acad. Sci.* **1091,** 517–530 (2006).
45. Askew, D. S., Ashmun, R. A., Simmons, B. C. & Cleveland, J. L. Constitutive c-myc expression in an IL-3-dependent myeloid cell line suppresses cell cycle arrest and accelerates apoptosis. *Oncogene* **6,** 1915–1922 (1991).
46. Evan, G. I. *et al.* Induction of apoptosis in fibroblasts by c-myc protein. *Cell* **69,** 119–128 (1992).
47. Matallanas, D. *et al.* Mutant K-Ras activation of the proapoptotic MST2 pathway is antagonized by wild-type K-Ras. *Mol. Cell* **44,** 893–906 (2011).
48. Pandit, B. *et al.* Gain-of-function RAF1 mutations cause Noonan and LEOPARD syndromes with hypertrophic cardiomyopathy. *Nat. Genet.* **39,** 1007–1012 (2007).
49. Razzaque, M. A. *et al.* Germline gain-of-function mutations in RAF1 cause Noonan syndrome. *Nat. Genet.* **39,** 1013–1017 (2007).
50. Kobayashi, T. *et al.* Molecular and clinical analysis of RAF1 in Noonan syndrome and related disorders: dephosphorylation of serine 259 as the essential mechanism for mutant activation. *Hum. Mutat.* **31,** 284–294 (2010).
51. Geiger, T., Wehner, A., Schaab, C., Cox, J. & Mann, M. Comparative proteomic analysis of eleven common cell lines reveals ubiquitous but varying expression of most proteins. *Mol. Cell. Proteom.* **11,** M111 014050 (2012).

© 2014 Macmillan Publishers Limited. All rights reserved.

METHODS

Cells. MCF7, HeLa, HEK293, NIH3T3 and mouse embryonic fibroblast (MEF) cells were grown in DMEM supplemented with 10% fetal calf serum (Gibco-BRL) and 2 mM L-glutamine (Gibco-BRL). Before each experiment, cells were serum starved overnight. Cells were transiently transfected using Lipofectamine 2000 (Invitrogen) following the manufacturer's protocol. MEFs were transfected using MEF transfection reagent (Altogen). Cell lines used were from ATCC and recently authenticated by STR profiling. Cells are internally tested every 6 weeks for mycoplasma contamination.

Disruptor peptides. The amino-terminal stearoylated MST2 peptide disruptor peptide Stear-IEELRQ**RYTAKRQPILDAMDAKK**RRQQNF (the minimal interacting interface as mapped by peptide arrays is shown in bold) and the scrambled sequence control peptide (Stear-TDKRALDQLRMQEIKARYPFQANRIRQKE) were synthesized by the Cancer Research UK Peptide Synthesis Laboratory.

Antibodies and reagents. Antibodies and reagents were from commercial sources. Mouse monoclonal anti-phospho-Ser-338 (catalogue number 05-534, Upstate, Millipore); rabbit polyclonal anti-phospho-Ser-473-Akt (catalogue number 9271), total anti-Akt (catalogue number 9272), anti-pS259 (catalogue number 9421), anti-phospho-MEK (catalogue number 9121), anti-total MEK (catalogue number 9122) and anti-HSP90 (catalogue number 4874) (Cell Signaling, NEB); mouse monoclonal anti-Raf1 (catalogue number 610152, clone 53), anti-MEK1 (catalogue number 610121, clone 25) and anti-MEK2 (catalogue number 610235, clone 96) (BD Transduction laboratories); goat polyclonal anti-Krs1/MST2 (C-19, catalogue number 6211), anti-LATS1 (G-16, catalogue number sc-12494) and anti-KSR1 (C-19, catalogue number sc-9317), mouse monoclonal anti-GAPDH (G-9, catalogue number sc365062) and rabbit polyclonal anti-14-3-3 (K-19, catalogue number sc-629) (Santa Cruz); rat monoclonal anti-HA–HRP (clone 3F10, catalogue number 12013819001) (Roche); mouse monoclonal anti-AU5 (discontinued from Sigma, now available from Abcam, clone AU5, catalogue number ab130113) (Abcam); monoclonal anti-Flag-M2-HRP (clone M2, catalogue number 8592); mouse monoclonal anti-phospho-ERK1/2 (clone MAPK-YT, catalogue number 8159) and rabbit polyclonal total ERK1/2 (catalogue number 5670) (Sigma-Aldrich); rabbit monoclonal anti-phospho-T180-Mst2 (clone EPR1467Y, catalogue number ab76323) and total anti-MST2 (clone EPR1466Y, catalogue number ab52641) (formerly Epitomics, Insight Biotech., now taken over by Abcam); mouse monoclonal anti-RASSF1A (clone eB114-10H1, catalogue number 14-6888-82) (eBioscience); mouse monoclonal anti-pan Ras (clone Ab-3, RAS10, catalogue number OP40) (Merck Millipore). Protein G–Sepharose- and anti-Flag-M2-conjugated agarose beads were from Sigma-Aldrich, PI(3)K inhibitor LY294002 and Akt inhibitor were from Calbiochem (Merck Biosciences), and MEK inhibitor U0126 was from Promega.

Recombinant proteins. Recombinant Raf-1 was from Sigma, MST2 and Akt from ProQinase and MEK from Millipore.

siRNAs. The following siRNAs: Scrambled (control), MEK1/2, RASSF1A, MST2 and LATS1 siRNAs were from Dharmacon, and were described previously[14].

Expression plasmids. pcDNA3.1–Flag–Raf1, point mutant S259A and pcDNA3.1–HA–RASSF1A were described previously[52,53]. pCEFL–AU5–Sos1, pCEFL–AU5–HRasV12 and the domain specific mutants (Ser 35, Cys 40) were provided by P. Crespo (Santander, Spain). pME18S–Flag–MST2 was previously described[10] and used to make kinase-dead mutant using the Quickchange mutagenesis kit (Stratagene). pcDNA3.1–Flag–LATS1 wild type and kinase dead mutant were gifts from X. Yang (Kingston, Canada).

Immunoprecipitations and immunoblotting. Cells were lysed on ice in 20 mM HEPES pH 7.5, NaCl 150 mM, 1% NP-40, 2 mM NaF, 10 mM β-glycerophosphate, 2 mM $Na_4P_2O_4$ and protease and phosphatase inhibitors. Lysates were cleared of debris by centrifugation at 10,000*g* for 20 min. Cleared lysates were incubated with respective antibodies for 4 h. Immunoprecipitates were washed three times in lysis buffer, separated by SDS–PAGE and analysed by western blotting as previously described[14]. Linear exposures of western blots were quantified by laser densitometry and the ImageJ software. The intensity of proteins co-precipitating with the bait was normalized to their corresponding expression in lysates and amount of immunoprecipitated bait. Similarly, phospho-proteins were normalized to the expression levels of the respective total protein. *y* axes show relative protein ratios or dimensionless scan units. Immunoprecipitations and immunoblots shown are representative of 3 or more independent experiments.

Kinase assays. MST2 activity was measured by in-gel kinase assays, which were performed using MST2 immunoprecipitates as previously described[10]. The Ser 259 phosphorylation assay was performed by incubating anti-Flag immunoprecipitates prepared from HEK293 cells overexpressing Flag-tagged constructs (LATS1 and MST2 wild type or kinase-dead mutants) in a kinase assay buffer consisting of 25 mM Tris-HCl (pH 7.5), 5 mM β-glycerophosphate, 2 mM dithiothreitol, 0.1 mM Na_3VO_4, 10 mM $MgCl_2$, 100 μM ATP and ~0.1 μg recombinant Raf-1 (Sigma R3652-1VL). Reactions were incubated for 30 min at 30 °C. Then, Raf-1 was immunoprecipitated from the assay mix and western blotted with pS259 antibody followed by anti-Raf-1 antibody.

Peptide array. Tricosanucleotide peptides overlapping by 5 amino acids and covering the full Raf-1 amino-acid sequence were immobilized on a nitrocellulose membrane and incubated with *in vitro* transcribed and translated ^{35}S-methionine-labelled MST2 protein. MST2 *in vitro* translation was performed using the cell-free TNT T7 Quick Coupled Transcription/Translation System from Promega. The membrane was washed and analysed by autoradiography.

Apoptosis assays. For analysis of apoptosis, attached and floating cells were collected, washed with PBS buffer, resuspended in 0.25% trypsin and fixed in 70% ethanol. Cells were then incubated with RNase (250 μg ml^{-1}, Qiagen) and stained with propidium iodide (10 μg ml^{-1}, Sigma) before analysis with a FACScalibur (Becton-Dickinson) or an AccuriC6 (Accuri Cytometers) flow cytometer. Apoptosis was determined by measuring DNA fragmentation to identify the SubG1 fraction. Results shown indicate fold increase in SubG1 population.

Cell proliferation. Cell proliferation was assayed using the CellTrace CFSE Cell Proliferation Kit (Molecular Probes) according to the manufacturer's protocol. Briefly, the CFSE fluorescent dye was added to the growth medium of cells for 15 min. At the times indicated in Fig. 6a cells were collected and washed with PBS before being analysed using an AccuriC6 flow cytometer. The assay measures the dilution of the fluorescent CFSE dye that occurs as a result of cell division and is proportional to cell doubling. The data were converted into growth curves as described previously[54].

Focus assays. NIH 3T3 cells were cultured in DMEM supplemented with 10% donor bovine serum, then were transfected with Lipofectamine (Invitrogen) according to the manufacturer's instructions. After 10–15 days, cells were fixed with 100% methanol and stained with Giemsa blue. Macroscopically visible foci were counted.

Colony-forming assays. NIH 3T3 cells were transfected using Lipofectamine and grown in the presence of 750 μg ml^{-1} G418 (Invitrogen). After 10 to 15 days, cells were fixed and stained, and colonies with a diameter greater than 2 mm were scored.

Zebrafish experiments. Zebrafish (*Danio rerio*) embryos were obtained from wild-type (AB strain) matings and maintained on a 14 h/10 h light/dark cycle at 28.5 °C. Five-hpf (hours post fertilization)-old embryos were incubated in embryo medium supplemented with various concentrations of the disruptor peptide and grown for 1 or 3 days. Dechorionated, deyolked[55] 24 hpf embryos were lysed for immunoblotting (5 embryos per lane). The pericardial areas of 3 dpf embryos (15 per condition) were photographed and measured using the ImageJ software. An area difference of >15% was scored as enlargement, and increases in heart size were between 19 and 23%. All zebrafish experiments were approved by the UCD Animal Research Ethics Committee.

Statistical methods. Statistical analyses were carried out using Excel using standard error of the mean (s.e.m.), and Student's *t*-test to calculate *P* values. A *P* value <0.05 was considered to be significant. No statistical method was used to pre-determine sample sizes for the zebrafish embryo experiments.

Mathematical models. Mathematical models were constructed using ordinary differential equations. Detailed descriptions, equations and parameters are included in the Supplementary Note. We also have provided a zipped Mathematica code file containing model equations that can be run using the Mathematica software.

52. Dent, P., Reardon, D. B., Morrison, D. K. & Sturgill, T. W. Regulation of Raf-1 and Raf-1 mutants by Ras-dependent and Ras-independent mechanisms *in vitro*. *Mol. Cell. Biol.* **15,** 4125–4135 (1995).
53. Ortiz-Vega, S. *et al.* The putative tumor suppressor RASSF1A homodimerizes and heterodimerizes with the Ras-GTP binding protein Nore1. *Oncogene* **21,** 1381–1390 (2002).
54. Luzyanina, T. *et al.* Numerical modelling of label-structured cell population growth using CFSE distribution data. *Theor. Biol. Med. Model.* **4,** 26 (2007).
55. Westerfield, M. *The Zebrafish Book. A Guide for the Laboratory Use of Zebrafish (Danio rerio)* 4th edn (Univ. Oregon Press, 2000).

© 2014 Macmillan Publishers Limited. All rights reserved.

DOI: 10.1038/ncb2986

nature cell biology

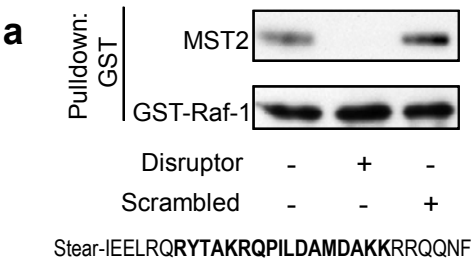

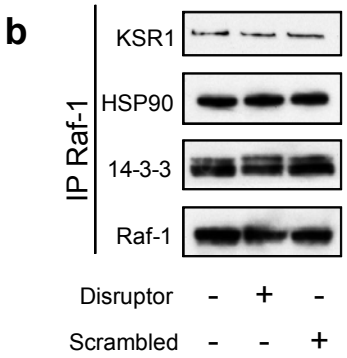

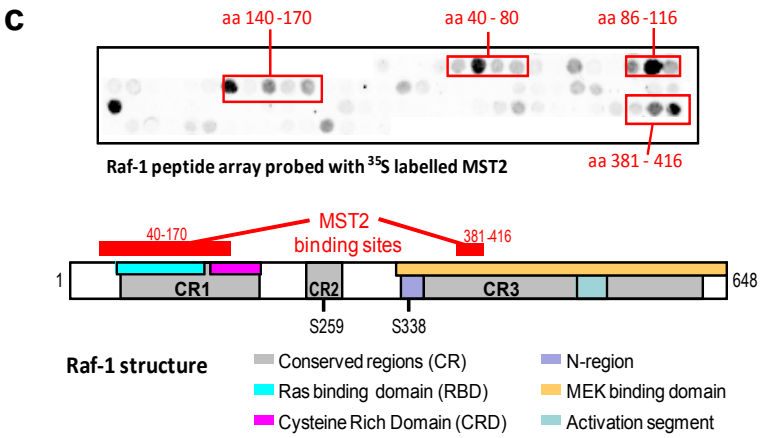

Supplementary Figure 1 The MST2 – Raf-1 interaction. **(a)** Disruption of the MST2 – Raf-1 protein complex by peptides *in vitro*. 10ng of purified GST-Raf-1 protein were incubated with 1µg of recombinant MST2 in the presence or absence of N-terminal stearylated disruptor or scrambled control peptides. GST pulldowns were analyzed by Western blotting as indicated. The sequence of the disruptor peptide is given below with the 17 amino acid interaction domain indicated in bold. **(b)** Co-immunoprecipitation of known Raf-1 interactors is not disturbed by the disruptor peptide. Serum starved HeLa cells were incubated with stearoylated-disruptor or scrambled control peptides. Raf-1 immunoprecipitates (IPs) were Western blotted for the known Raf-1 binding proteins KSR1, HSP90, and 14-3-3. **(c)** Mapping of the MST2 interaction sites on Raf-1. The Raf-1 amino acid sequence was synthesized as a set of 23mer peptides overlapping by 5 amino acids that were immobilised on a nitrocellulose membrane. The membrane was probed with a ^{35}S-methionine labelled MST2 protein that was produced by coupled *in vitro* transcription translation as described in the methods section. MST2 binding peptides in the Raf-1 sequence are boxed in red, and the MST2 binding sites are indicated on the schematic Raf-1 structure.

© 2014 Macmillan Publishers Limited. All rights reserved.

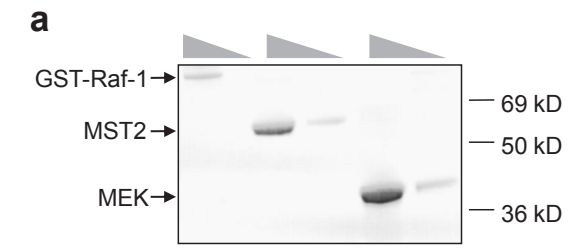

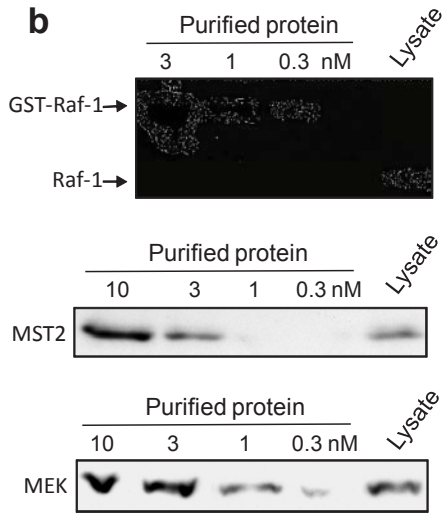

Proteins	Hela	MCF7
Raf-1	0.6 μM	0.8 μM
MEK	1.73 μM	2.31 μM
MST2	2.15 μM	2.07 μM

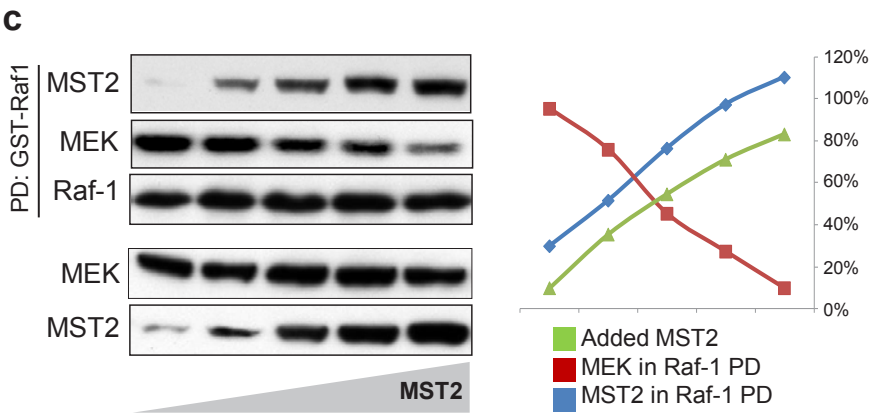

Supplementary Figure 2 Protein concentrations and effects on Raf-1 binding to MST2 or MEK. **(a,b)** Determination of Raf-1, MEK and MST2 protein concentrations by quantitative Western blotting. **(a)** Coomassie stained gel of purified, recombinant proteins used as standards. **(b)** Examples of Western blots where the concentrations of Raf-1, MEK, and MST2 in MCF7 cells were determined by comparison of the signal obtained in cell lysates against respective purified protein standards of known concentrations. Blots were quantified by laser densitometry and analysed using the NIH Image J software. The standards were used to generate a reference curve, and the concentration of the proteins in the cell lysates were calculated after adjustment for the dilution during cell lysis. The table shows protein concentrations per cell assuming a cell volume of 1pL. **(c)** MST2 and MEK compete for Raf-1 binding in vitro. 1ng of recombinant GST-tagged Raf-1 was incubated in vitro with 2ng of recombinant MEK and increasing amounts (0.01-2ng) of recombinant MST2. GST pulldowns and total levels of proteins were analyzed by Western blot using antibodies against the indicated proteins. Blots were quantified by laser densitometry as above.

© 2014 Macmillan Publishers Limited. All rights reserved.

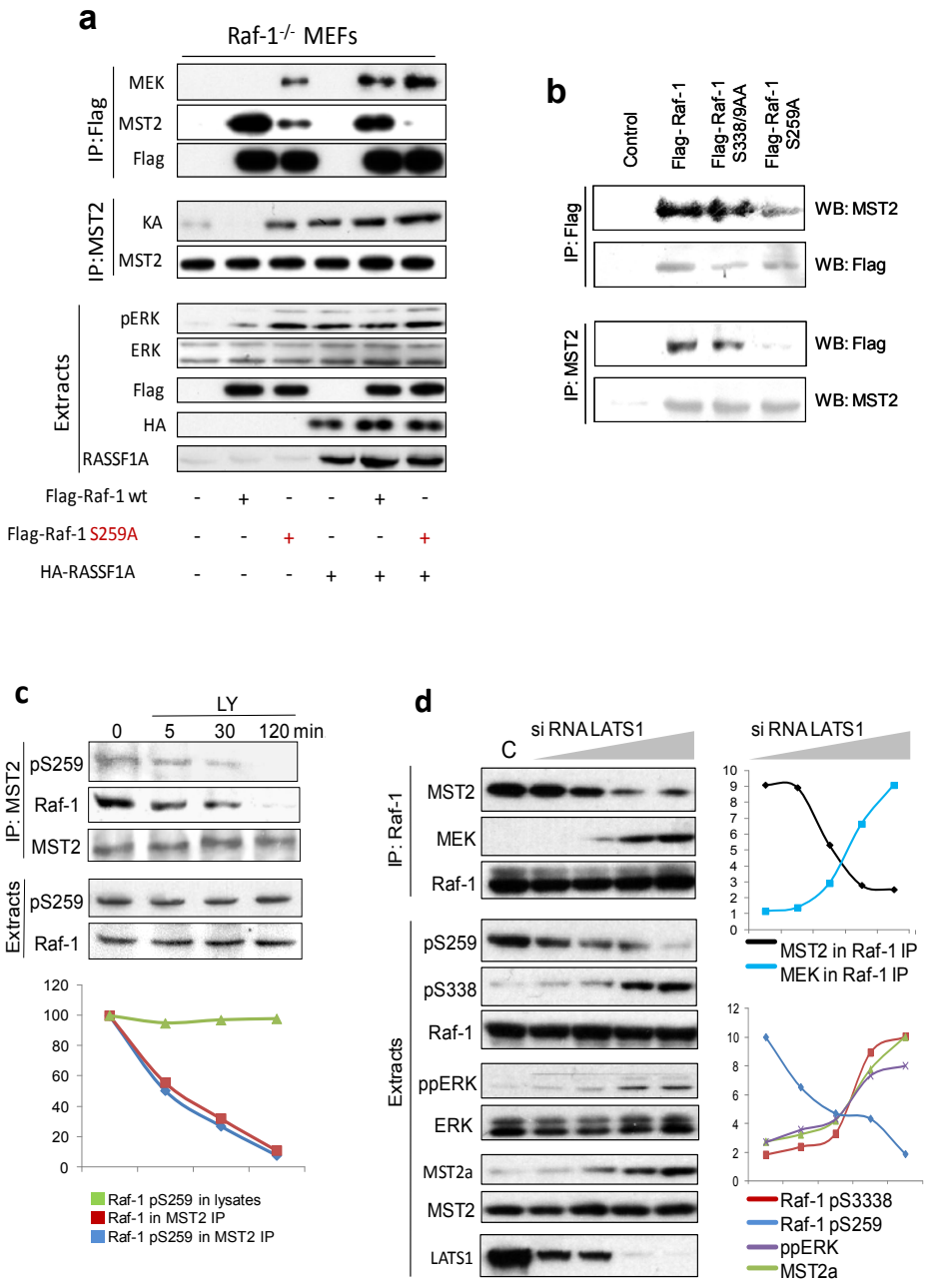

Supplementary Figure 3 The role of Raf-1 S259 phosphorylation. **(a)** Simultaneous activation of Raf-1 and MST2 signaling by S259 dephosphorylation and RASSF1A. Raf-1$^{-/-}$ MEFs were co-transfected with either wild type (wt) Flag-Raf-1 or the Flag-Raf-1 S259A mutant and HA-RASSF1A as indicated. Flag-IPs were analyzed by Western blotting using antibodies against the indicated proteins. MST2 kinase activity was assayed from MST2 IPs by an in gel kinase assay as described in the Methods section. 10µg of cell extracts were blotted using antibodies against phospho- or total proteins as indicated. **(b)** Mutation of S338/339 in Raf-1 does not affect binding to MST2. MCF7 cells were co-transfected with Flag-Raf-1 or the Flag-Raf-1 SS338/9 or S259A mutants as indicated. Flag-IPs were blotted for associated MST2 and MST2 IPs were blotted with Flag antibody. **(c)** Inhibition of phosphoinositide-3 kinase (PI3K) does not affect Raf-1 phosphorylation on S259. MCF7 cells were treated with 10µM PI3K inhibitor LY294002 (LY) for the indicated times. MST2 IPs were examined for associated Raf-1 and phosphorylation of S259 in Raf-1. 10µg cell extracts were blotted for Raf-1 and pS259. Blots were quantified as above. The graph shows the S259 phosphorylation in extracts normalized to Raf-1 levels in the extracts; and the Raf-1 and pS259 signals in MST2 IPs normalized to the levels of MST2, or Raf-1 and MST2 contained in the IPs, respectively. The dissociation of the MST2 – Raf-1 complex is due to the inhibition of Akt mediated MST2 phosphorylation, which enhances the binding of MST2 to Raf-1.[1] **(d)** LATS1 downregulation induces a switch-like change from MST2-Raf-1 to MEK-Raf-1 complexes and an activation of Raf-1, ERK and MST2. Hela cells were transfected with increasing concentration of LATS1 (0-100nM) or scrambled control (C) siRNAs. Raf-1 and MST2 IPs and 10µg of cellular extracts were analyzed by Western blotting for the indicated phospho- and total proteins. Blots were quantitated by laser densitometry and analysed using the Image J software. Corresponding simulations are shown in Fig. M8.

© 2014 Macmillan Publishers Limited. All rights reserved.

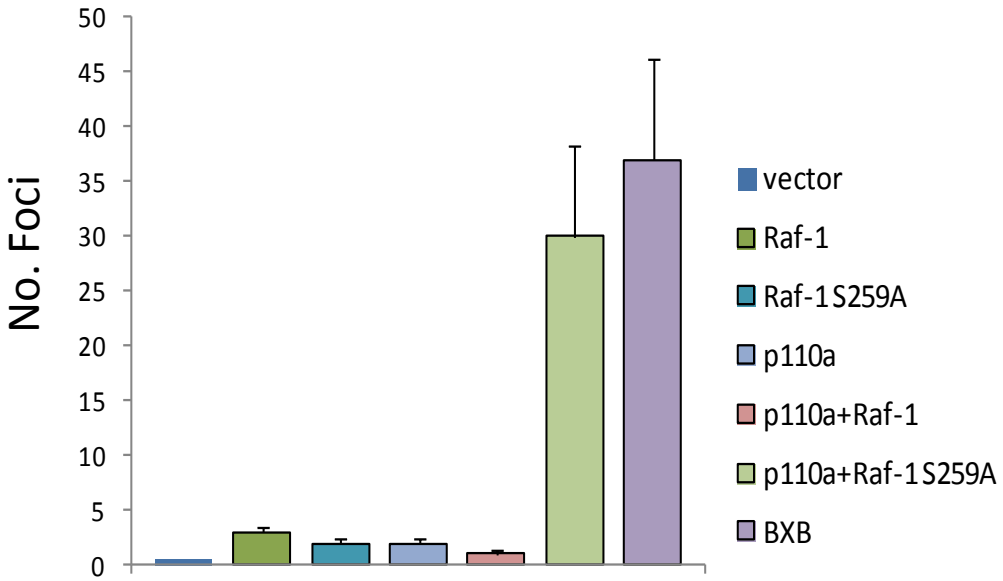

Supplementary Figure 4 Activated PI3 kinase synergises with the Raf-1 S259A in cell transformation. NIH3T3 cells were transfected with the indicated constructs, allowed to grow to confluence and assayed for focus formation 2 weeks after transfection. p110a is the catalytic subunit of PI3Kα rendered constitutively active by fusion to a myristylation signal. BXB is the truncated Raf-1 kinase domain, which functions as oncogene.[2] Error bars represent SEM, n=4.

© 2014 Macmillan Publishers Limited. All rights reserved.

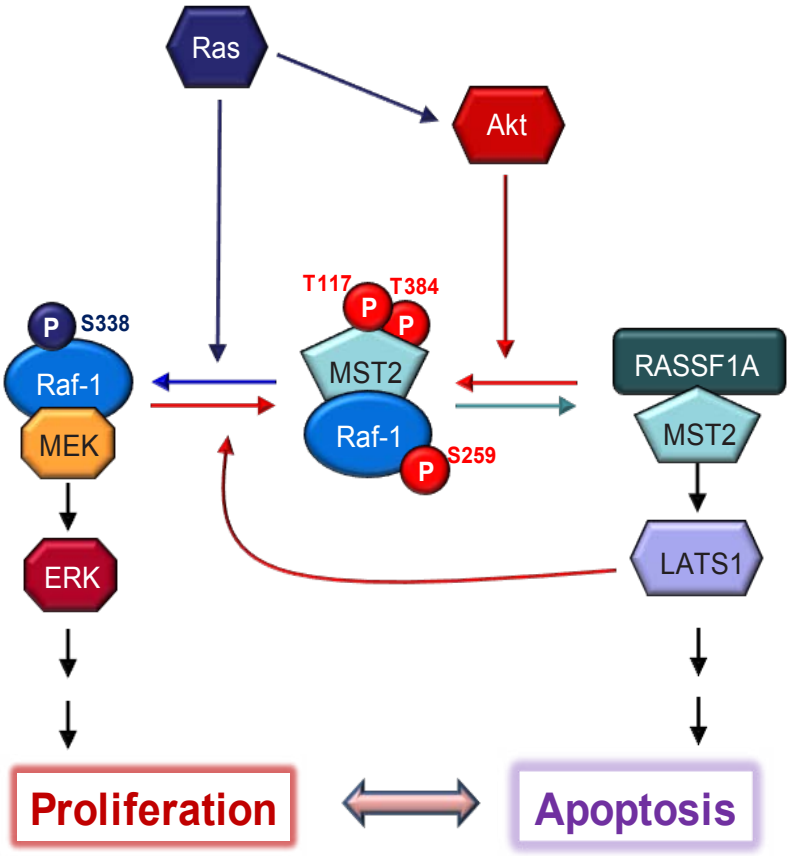

Supplementary Figure 5 Schematic summary. Switch-like transitions between Raf-1 binding to MST2 or MEK determine biological outcomes such as proliferation versus apoptosis.

© 2014 Macmillan Publishers Limited. All rights reserved.

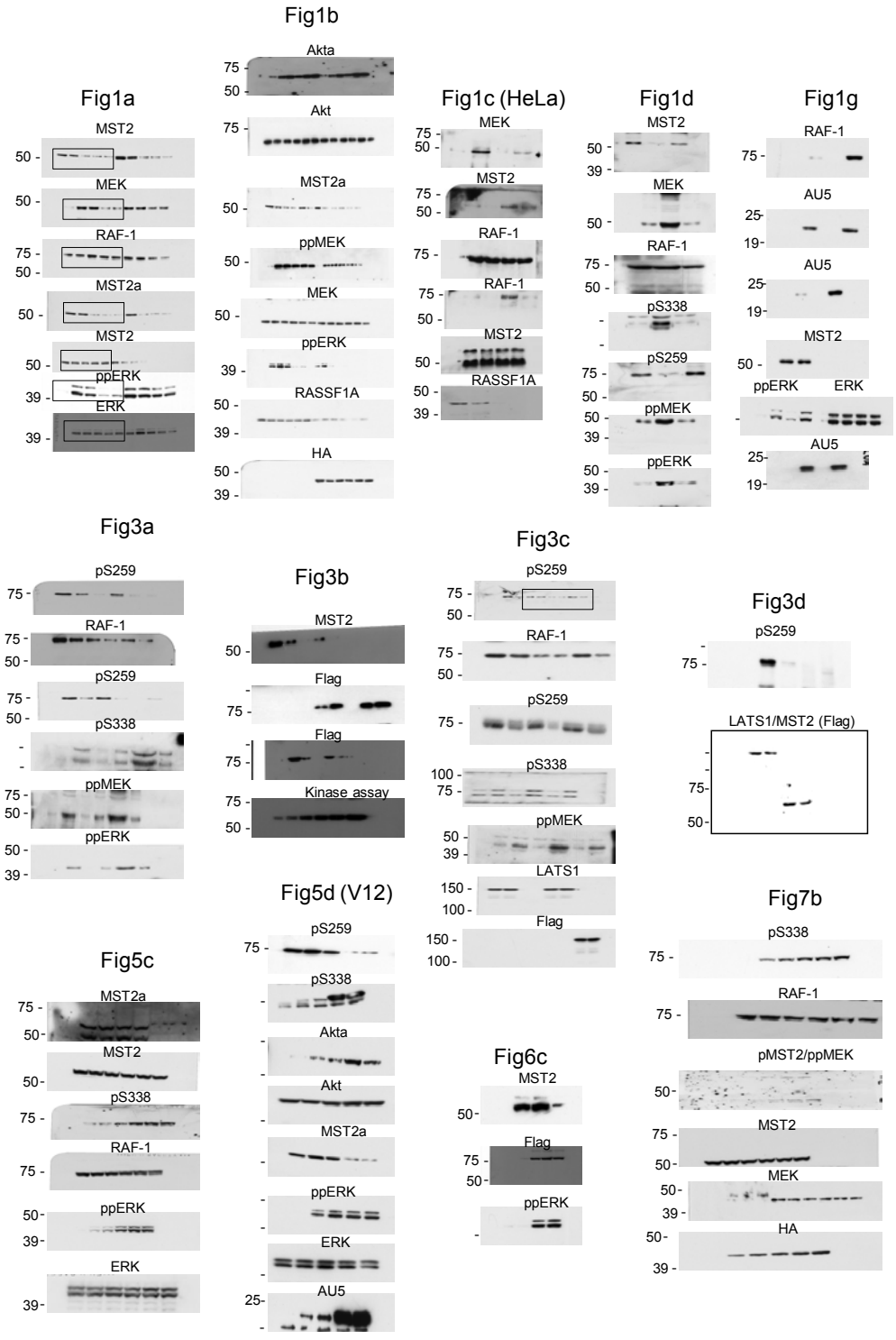

Supplementary Figure 6 Uncropped images of films of key experiments.

© 2014 Macmillan Publishers Limited. All rights reserved.

References

1. Romano, D. *et al.* Proapoptotic kinase MST2 coordinates signaling crosstalk between RASSF1A, Raf-1, and Akt. *Cancer research* **70**, 1195-1203 (2010).
2. Heidecker, G. *et al.* Mutational activation of c-raf-1 and definition of the minimal transforming sequence. *Molecular and cellular biology* **10**, 2503-2512 (1990).

© 2014 Macmillan Publishers Limited. All rights reserved.

Supplementary Note

Mathematical Models

1. Construction and analysis of the generic core models for protein complexes formed by competing interaction partners

Our combined experimental data suggest that competing protein complexes can function as molecular switches that distribute signals from one pathway into another. Here, we present the computational analysis of two different generic models of competing protein complexes.. In the first model, the competing binding partners have only one affinity state, whereas in the second model each binding partner can be in a high or low affinity state. Our aim is to analyse conditions which could lead to a pronounced switching behaviour.

1.1 Generic model of simple binding interaction with single-state binding partners

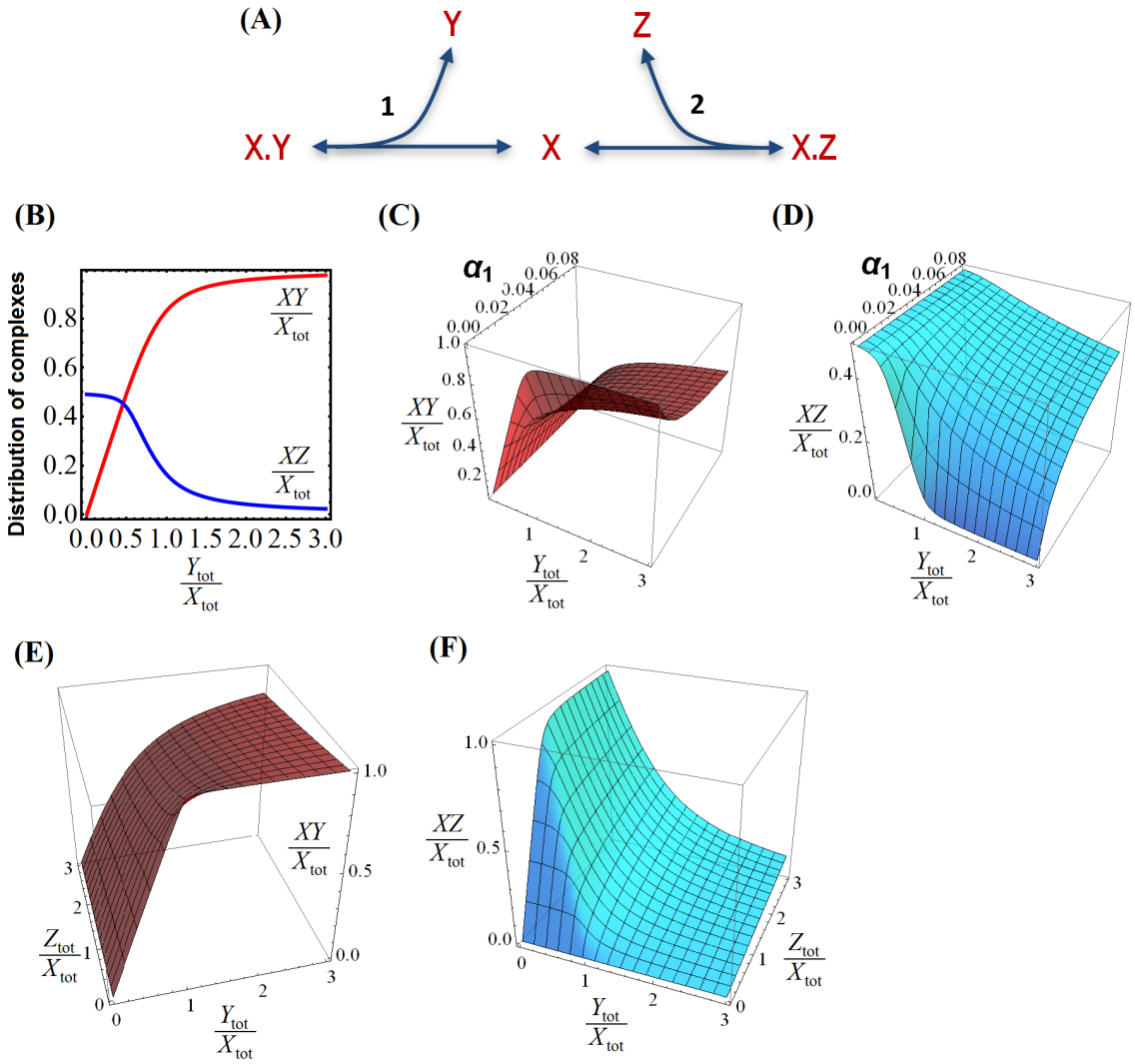

Figure M1. Scheme and analysis of the simple binding interaction model. **(A)** Scheme of protein-protein interactions between protein X and two binding partners Y and Z. **(B,C,D)** Switch-like behaviour of the binding competition system shown in Fig.M1A. Italic notation denotes the concentration of the respective molecular species. **(B)** Dependence

© 2014 Macmillan Publishers Limited. All rights reserved.

of the steady-state levels of bound protein fraction *XY* and *XZ* on Y_{tot}/X_{tot}. α_1 and α_2 are the dissociation constants of the complexes XY and XZ normalized by the total concentration of X, X_{tot} (see text). Parameter values are $\alpha_1 = 0.001$, $\alpha_2 = 0.01$, $Z_{tot}/X_{tot} = 0.5$. **(C)** Dependence of the steady-state level of bound protein fraction *XY* on Y_{tot}/X_{tot} and α_1. **(D)** Dependence of the steady-state level of bound protein fraction *XZ* on Y_{tot}/X_{tot} and α_1. Parameter values used for panel C, D are $\alpha_2 = 0.01$ and $Z_{tot}/X_{tot} = 0.5$. **(E,F)** Dependence of the steady-state levels of bound protein fraction **(E)** *XY* and **(F)** *XZ* on Y_{tot}/X_{tot} and Z_{tot}/X_{tot}. Parameter values used are $\alpha_1 = 0.001$, $\alpha_2 = 0.01$.

In this generic model (schematised in Fig. M1A) we assume that protein X can reversibly bind to (and dissociate from) protein Y or Z and can therefore exist in either free form, or in the complex with Y or Z. We now explore dynamic transition between these different forms of X and seek conditions under which switching behaviour may occur.

Using the species names (*X, Y, Z, XY, XZ*) to indicate their corresponding concentration levels, at the steady state (which is the chemical equilibrium), we have

$$XY = \frac{X \cdot Y}{K_Y} \text{ and } XZ = \frac{X \cdot Z}{K_Z} \quad (1)$$

where K_Y and K_Z are the dissociation constants of reactions 1 and 2, respectively.

The total abundances of *X, Y* and *Z* are assumed constant and denoted as X_{tot}, Y_{tot} and Z_{tot}. Using the law of conservation, we have:

$$\begin{aligned} X_{tot} &= X + XZ + XY \\ Y_{tot} &= Y + XY \\ Z_{tot} &= Z + XZ \end{aligned} \quad (2)$$

For convenience of analysis, we performed dimensionless transformation to transform the state variables and parameters into dimensionless forms, as follows.

$$x = \frac{X}{X_{tot}},\ y = \frac{Y}{Y_{tot}},\ z = \frac{Z}{Z_{tot}},\ r_1 = \frac{Y_{tot}}{X_{tot}},\ r_2 = \frac{Z_{tot}}{X_{tot}},\ \alpha_1 = \frac{K_Y}{X_{tot}}; \alpha_2 = \frac{K_Z}{X_{tot}} \quad (3)$$

where *x*, *y* and *z* represent the *X, Y, Z* protein concentrations normalized by their respective abundance. The parameters r_1 and r_2 compare the relative abundances of proteins *Y* and *Z* to that of *X*; and α_1 and α_2 represent the dissociation constants of the complexes *XY* and *XZ* normalized by X_{tot}.

© 2014 Macmillan Publishers Limited. All rights reserved.

Equations (2) can be rewritten as:

$$1 = x + \frac{XZ}{X_{\text{tot}}} + \frac{XY}{X_{\text{tot}}}$$
$$1 = y + \frac{XY}{Y_{\text{tot}}} \qquad (4)$$
$$1 = z + \frac{XZ}{Z_{\text{tot}}}$$

Eqn. (3) and (1) lead to:

$$\frac{XY}{X_{\text{tot}}} = \frac{1}{X_{\text{tot}}}\frac{X \cdot Y}{K_Y} = x \cdot y \cdot \frac{Y_{\text{tot}}}{K_Y} = x \cdot y \cdot \frac{Y_{\text{tot}}}{X_{\text{tot}}}\frac{X_{\text{tot}}}{K_Y} = x \cdot y \cdot \frac{r_1}{\alpha_1}$$
$$\frac{XY}{Y_{\text{tot}}} = \frac{1}{Y_{\text{tot}}}\frac{X \cdot Y}{K_Y} = x \cdot y \cdot \frac{X_{\text{tot}}}{K_Y} \quad \frac{x \cdot y}{\alpha_1}$$
$$\frac{XZ}{X_{\text{tot}}} = \frac{1}{X_{\text{tot}}}\frac{X \cdot Z}{K_Z} = x \cdot z \cdot \frac{Z_{\text{tot}}}{K_z} = x \cdot z \cdot \frac{Z_{\text{tot}}}{X_{\text{tot}}}\frac{X_{\text{tot}}}{K_z} = x \cdot z \cdot \frac{r_2}{\alpha_2}$$
$$\frac{XZ}{Z_{\text{tot}}} = \frac{1}{Z_{\text{tot}}}\frac{X \cdot Z}{K_Z} = x \cdot z \cdot \frac{X_{\text{tot}}}{K_Z} \quad \frac{x \cdot z}{\alpha_2}$$

Substitution of these components into eqn. (4) yields:

$$1 = x + x \cdot y \cdot \frac{r_1}{\alpha_1} + x \cdot z \cdot \frac{r_2}{\alpha_2}$$
$$1 = y + \frac{x \cdot y}{\alpha_1} = y\left(1 + \frac{x}{\alpha_1}\right) \qquad (5)$$
$$1 = z + \frac{x \cdot z}{\alpha_2} = z\left(1 + \frac{z}{\alpha_2}\right)$$

Putting $y = \frac{\alpha_1}{x + \alpha_1}$ and $z = \frac{\alpha_2}{x + \alpha_2}$ into the first equation of (5) means that the steady-state solutions can be obtained by solving the following equation:

$$1 = x + \frac{r_1 \cdot x}{\alpha_1 + x} + \frac{r_2 \cdot x}{\alpha_2 + x} \qquad (6)$$

The three components in the right hand side of eqn. (6) represent, respectively, the free and bound protein fractions of *X* with *Y* and *Z*, normalized by the total *X* abundance (X_{tot}).

We solved equation (6) and simulated the system for a variety of parameter regimes. Under selected conditions, the system demonstrates switch-like behaviour as shown in Fig. M1. As the relative abundance of *Y* gradually increases, an off-switch is observed for steady-state level of *X* bound to *Z*, accompanied by a saturating but not switch-like increase of *X* bound to *Y* (Fig. M1B). Similarly, an off-switch for *XY* is observed if the input is an increase in the relative abundance of *Z* (data not shown). Further analysis showed that the switch-like response observed for *XZ* as displayed in Fig. M1D is more pronounced at small α_1, i.e. when *Y* has strong binding affinity for *X*. Under weak *XY* association or strong dissociation, switch-like behaviour is compromised (Fig. M1C,D). When considering both r_1 and r_2 as inputs, the

© 2014 Macmillan Publishers Limited. All rights reserved.

XZ off-switch becomes more pronounced if *Z* is much less abundant compared to *X*. However, when *Z* is much more abundant than *X*, the decrease of *XZ* becomes graded (Fig. M1E,F).

The simulations above indicate that only if the affinities of *Y* and *Z* are very different, raising the concentration of the high affinity binder induces a steep non-linear decrease in the protein complex between *X* and the low-affinity binder. Otherwise, the transitions between *XY* and *XZ* are smooth. To further substantiate this statement, let us consider the case when the affinities of *Y* and *Z* for binding *X* are comparable. Assuming $\alpha_1 = \alpha_2$, eqn. (6) now becomes:

$$1 = x\left(1 + \frac{r_1 + r_2}{\alpha_1 + x}\right)$$

Or $$x^2 + (\alpha_1 + r_1 + r_2 - 1)\cdot x - \alpha_1 = 0$$

This equation has only one positive root for *x* which is:

$$x = 1 - \alpha_1 - r_1 - r_2 + \sqrt{4\alpha_1 + (1 - \alpha_1 - r_1 - r_2)^2}$$

The bound protein fractions of *X* with *Y* and *Z*, normalized by the total *X* can be computed from eqn. (6). When plotting the *XZ* and *XY* fractions against increasing *Y* abundance (r_1), we found that the transitions between *XZ* and *XY* are always smooth for all values of α_1 and r_2. This further supports that abrupt transition between protein complexes can only be observed when the affinities of *Y* and *Z* for *X* are significantly different.

1.2. Covalent modifications of interacting proteins resulting in high- or low affinity states bring about switch-like digital outputs

Here we modified the simple binding interaction model to include the possibility that competing binding partners may exist in two states, a high and a low affinity state generated through enzymatic modification, e.g. phosphorylation (Fig. M2A). We assume that protein X with the high affinity for Y can be modified into low affinity state X_1 (reaction 1), which can be converted back to X (reaction 2). As an example, X and X_1 may represent the unphosphorylated and phosphorylated forms of a protein. A similar cycle affects protein Y through reactions 3 and 4. We assume that only high-affinity forms X and Y bind to each other. Consequently, the modification cycles of X and Y are linked via formation of the XY complex by reversible binding between X and Y (reaction 5). For illustrative purposes, we assume that X_1 and Y_1 can associate with different protein binding partners A and B, respectively and the binding complexes can potentially elicit distinct downstream signalling effects. Importantly, this core network resembles a simplified circuit of the Raf-1/MST2 pathway considered in Fig.4, where X, Y, A and B represent inactive MST2, inactive Raf-1 (phosphorylated on S259), RASSF1A and MEK, respectively. We will show here that such molecular circuitry demonstrates switching behaviour and can convert graded, analogue inputs into switch-like, digital outputs.

Following Michaelis-Menten kinetic law, the reaction rates of reactions 1-4 in Fig.M2A are formulated as follows:

$$v_1 = V_1\frac{X}{K_1 + X},\ v_2 = V_2\frac{X_1}{K_2 + X_1}, v_3 = V_3\frac{Y}{K_3 + Y},\ v_4 = V_4\frac{Y_1}{K_4 + Y_1}.$$

© 2014 Macmillan Publishers Limited. All rights reserved.

When the system reaches a steady state, we have:

$$v_5 = v_6 = v_7 = 0 \quad (7a)$$

$$v_1 = v_2 . \quad (7b)$$

$$v_3 = v_4 \quad (7c)$$

The total abundances of X, Y, A and B are assumed constant and denoted as X_{tot}, Y_{tot}, A_{tot} and B_{tot}. Conservation laws give:

$$X + XY + X_1 + X_1 A = X_{\text{tot}} \quad (8a)$$

$$Y + XY + Y_1 + Y_1 B = Y_{\text{tot}} \quad (8b)$$

$$A + X_1 A = A_{\text{tot}} \quad (8c)$$

$$B + Y_1 B = B_{\text{tot}} \quad (8d)$$

We introduce the following dimensionless concentrations and parameters:

$$x = \frac{X}{X_{\text{tot}}}, y = \frac{Y}{Y_{\text{tot}}}, \; x_1 = \frac{X_1}{X_{\text{tot}}}, \; y_1 = \frac{Y_1}{Y_{\text{tot}}}, xy = \frac{XY}{X_{\text{tot}}}, a = \frac{A}{X_{\text{tot}}}, b = \frac{B}{Y_{\text{tot}}}$$

$$r = \frac{Y_{\text{tot}}}{X_{\text{tot}}}, r_a = \frac{A_{\text{tot}}}{X_{\text{tot}}}, r_b = \frac{B_{\text{tot}}}{Y_{\text{tot}}},$$

$$\alpha_d = \frac{K_d}{X_{\text{tot}}}, \alpha_a = \frac{K_a}{X_{\text{tot}}}, \alpha_b = \frac{K_b}{Y_{\text{tot}}},$$

$$\kappa_1 = \frac{K_1}{X_{\text{tot}}}, \; \kappa_2 = \frac{K_2}{X_{\text{tot}}}, \kappa_3 = \frac{K_3}{Y_{\text{tot}}}, \; \kappa_4 = \frac{K_4}{Y_{\text{tot}}}$$

The dimensionless variables x, x_1, xy and a represent the X, X_1, the complex XY and A protein concentrations normalized by the abundance of X. The variables y, y_1 and b represent the Y, Y_1, and B protein concentrations normalized by the abundance of Y. The parameters r, r_a and r_b compare the relative abundances of Y and A to that of X, and B to that of Y. $\alpha_d, \alpha_a, \alpha_b$ denotes the dimensionless dissociation constant of the complex XY, X_1A normalized by X_{tot}, and Y_1B normalized by Y_{tot} which describes how strong the binding is (or how abundant the high affinity state is). The parameters $\kappa_1, \kappa_2, \kappa_3$ and κ_4 are the dimensionless Michaelis-Menten constants of the reactions 1-4, normalized by X_{tot} and Y_{tot}.

Eqn. (7a) gives:

$$x + x_1 + \frac{XY}{X_{\text{tot}}} + \frac{X_1 A}{X_{\text{tot}}} = 1 \quad (9)$$

Since v_5=0 and v_6=0 we have

© 2014 Macmillan Publishers Limited. All rights reserved.

$$\frac{XY}{X_{\text{tot}}} = \frac{1}{X_{\text{tot}}}\frac{X \cdot Y}{K_d} = \frac{(X/X_{\text{tot}})\cdot(Y/Y_{\text{tot}})}{K_d/X_{\text{tot}}}\cdot\frac{Y_{\text{tot}}}{Y_{\text{tot}}} = \frac{x\cdot y}{\alpha_d}\cdot\frac{Y_{\text{tot}}}{X_{\text{tot}}} = x\cdot y\cdot\frac{r}{\alpha_d}$$

$$\frac{X_1 A}{X_{\text{tot}}} = \frac{1}{X_{\text{tot}}}\frac{X_1 \cdot A}{K_a} = \frac{(X_1/X_{\text{tot}})\cdot(A/X_{\text{tot}})}{K_a/X_{\text{tot}}} = \frac{x_1\cdot a}{\alpha_a}$$

Substitute these into (9) we have:

$$x_1\left(1+\frac{a}{\alpha_a}\right) = 1 - x\left(1+y\cdot\frac{r}{\alpha_d}\right) \tag{10}$$

Next, divide both sides of the conservation law (8c) by X_{tot} and substitute $X_1 A$ derived above in, we have:

$$a + \frac{x_1\cdot a}{\alpha_a} = r_a \Leftrightarrow a = \frac{r_a}{1+x_1/\alpha_a}$$

Eqn. (10) then becomes:

$$x_1\left(1+\frac{r_a}{x_1+\alpha_a}\right) = 1 - x\left(1+y\cdot\frac{r}{\alpha_d}\right) \tag{11}$$

Apply similar derivation for *Y*-related species, we have eqn. (7b) is equivalent to:

$$y + y_1 + \frac{XY}{Y_{\text{tot}}} + \frac{Y_1 B}{Y_{\text{tot}}} = 1 \tag{12}$$

Since v_5=0 and v_7=0 we have

$$\frac{XY}{Y_{\text{tot}}} = \frac{1}{Y_{\text{tot}}}\frac{X\cdot Y}{K_d} = \frac{(X/X_{\text{tot}})\cdot(Y/Y_{\text{tot}})}{K_d/X_{\text{tot}}} = \frac{x\cdot y}{\alpha_d}$$

$$\frac{Y_1 B}{Y_{\text{tot}}} = \frac{1}{Y_{\text{tot}}}\frac{Y_1\cdot B}{K_b} = \frac{(Y_1/Y_{\text{tot}})\cdot(B/Y_{\text{tot}})}{K_b/Y_{\text{tot}}} = \frac{y_1\cdot b}{\alpha_b}$$

Substitute these into (12) and rearrange we get:

$$y_1\left(1+\frac{b}{\alpha_b}\right) = 1 - y\left(1+\frac{x}{\alpha_d}\right) \tag{13}$$

Next, divide both sides of the conservation law (8d) by Y_{tot} and substitute $Y_1 B$ derived above in, we have:

$$b = \frac{r_b}{1+y_1/\alpha_b}$$

Eqn. (13) then becomes:

$$y_1\left(1+\frac{r_b}{y_1+\alpha_b}\right) = 1 - y\left(1+\frac{x}{\alpha_d}\right) \tag{14}$$

© 2014 Macmillan Publishers Limited. All rights reserved.

We can then solve the quadratic eqns. (13) and (14) for x_1 and y_1 which are obtained as positive functions of x, y and the other parameters as below.

$$x_1 = \frac{1}{2\alpha_d}\left(C + \sqrt{C^2 - 4\alpha_d \cdot D}\right) \tag{15}$$

$$y_1 = \frac{1}{2\alpha_d}\left(E + \sqrt{E^2 - 4\alpha_d \cdot F}\right) \tag{16}$$

where

$$C = \alpha_d - \alpha_a \cdot \alpha_d - \alpha_d \cdot r_a - \alpha_d \cdot x - r \cdot x \cdot y$$
$$D = -\alpha_a \cdot \alpha_d + \alpha_a \cdot \alpha_d \cdot x + \alpha_a \cdot r \cdot x \cdot y$$
$$E = \alpha_d - \alpha_b \cdot \alpha_d - \alpha_d \cdot r_b - x \cdot y$$
$$F = -\alpha_b \cdot \alpha_d + \alpha_b \cdot \alpha_d \cdot y + \alpha_b \cdot x \cdot y$$

Note that

$$v_1 = V_1 \frac{X}{K_1 + X} = V_1 \frac{x}{\kappa_1 + x},\ v_2 = V_2 \frac{X_1}{K_2 + X_1} = V_2 \frac{x_1}{\kappa_2 + x_1}$$
$$v_3 = V_3 \frac{Y}{K_3 + Y} = V_3 \frac{y}{\kappa_3 + y},\ v_4 = V_4 \frac{Y_1}{K_4 + Y_1} = V_4 \frac{y_1}{\kappa_4 + y_1}$$

The steady-state condition (7b) and (7c) means

$$V_1 \frac{x}{\kappa_1 + x} = V_2 \frac{x_1}{\kappa_2 + x_1} \text{ and } V_3 \frac{y}{\kappa_3 + y} = V_4 \frac{y_1}{\kappa_4 + y_1}.$$

Substituting (10) into these equation yields

$$\left(\frac{V_1}{V_2}\right)\frac{x}{\kappa_1 + x} = \frac{\frac{1}{2\alpha_d}\left(C + \sqrt{C^2 - 4\alpha_d \cdot D}\right)}{\kappa_2 + \left(\frac{1}{2\alpha_d}\left(C + \sqrt{C^2 - 4\alpha_d \cdot D}\right)\right)} \tag{17}$$

$$\left(\frac{V_3}{V_4}\right)\frac{y}{\kappa_3 + y} = \frac{\frac{1}{2\alpha_d}\left(E + \sqrt{E^2 - 4\alpha_d \cdot F}\right)}{\kappa_4 + \left(\frac{1}{2\alpha_d}\left(E + \sqrt{E^2 - 4\alpha_d \cdot F}\right)\right)} \tag{18}$$

The steady-state solutions for x and y can now be obtained by solving the Eqns. (17-18). The steady-state solutions for x_1 and y_1 can then be obtained using (15-16). Finally, the steady-state solutions for the relative complex XY/X_{tot}, X_1A/X_{tot} and Y_1B/Y_{tot} can then be computed as $x \cdot y \cdot \frac{r}{\alpha_d}$, $\frac{x_1 \cdot r_a}{x_1 + \alpha_a}$ and $\frac{y_1 \cdot r_b}{y_1 + \alpha_b}$, respectively.

We found that the system displays steep switching transitions between the proteins states (Fig. M2B). The existence of sharp switches relies on the degree of saturation of the

© 2014 Macmillan Publishers Limited. All rights reserved.

participating reactions, characterised by the respective Michaelis-Menten constants (κ_1, κ_2, κ_3 , κ_4). Fig. M2E demonstrate that switch-like behaviours are prominent when the reactions 1-4 are under saturating condition (low κ_d, here assumed as a common value for all κ_1, κ_2, κ_3 , κ_4), while less pronounced when the reactions are far from the saturating regime. Under proper condition, overexpression of a protein binding partner such as A results in enhanced levels of both complexes X_1A and Y_1B and decreased levels of XY binding (Figs. M2C,D). Similar behaviours were also observed in response to overexpression of B (not shown). Furthermore, as follows from eqns. 11 and 12, the level of cross-talk between two pathways, characterised by the dissociation constant (α_d) of the *XY* binding reaction, also affects how the switches are realised. Our simulations showed that while the switches for x_1 and y_1 are persistent at a wide range of α_d, the response of y_1 becomes less significant at very low α_d (data not shown). This means that exceedingly strong affinity between *X* and *Y* can weaken the switch-like behaviour of y_1 in response to V_1/V_2 and of x_1 in response to V_3/V_4.

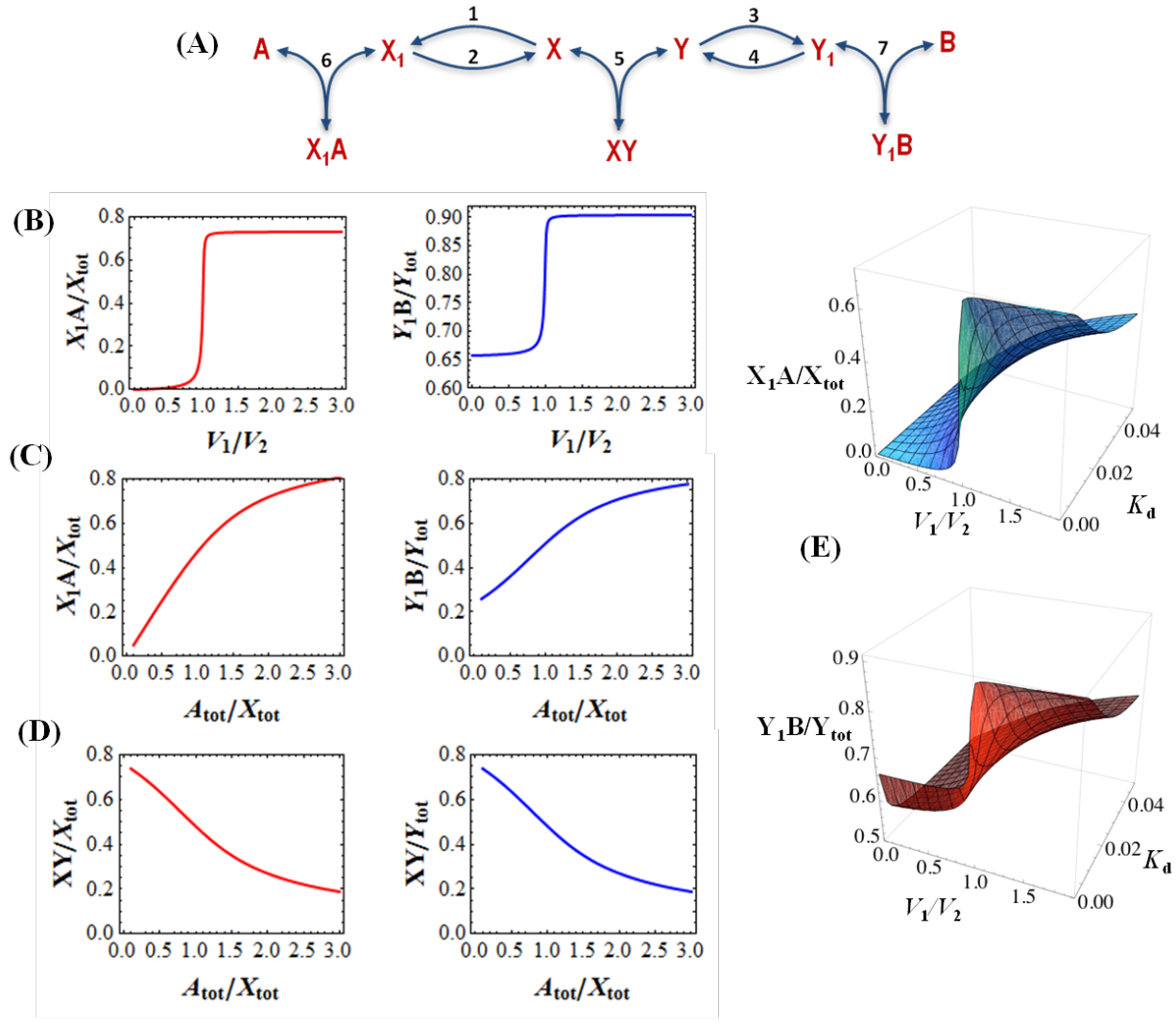

Fig. M2: Scheme and analysis of a two affinity-state interaction model.
(A) Scheme of protein complex formation where the binding partners exist in high and low affinity interaction states that are determined by post-translational modifications. **(B)** Protein modifications can convert graded, analogue inputs into digital outputs. Dependence of the steady-state levels of x_1 and y_1 on the ratio of maximum rate constants V_1/V_2. Parameter values are $\kappa_1 = \kappa_2 = \kappa_3 = \kappa_4 = 0.001$, $r = 2$, $r_a = r_b = 1$, $\alpha_d = 0.001$, $\alpha_a = 0.1$, $\alpha_b = 0.01$ and $V_3/V_4 = 2$.

© 2014 Macmillan Publishers Limited. All rights reserved.

(C,D) Effects of overexpression of protein A on relevant protein complexes. Dependence of the steady-state levels of the relative concentrations of **(C)** X_1A, Y_1B and **(D)** XY on increasing abundance of the binding partner A. Parameter values are $\kappa_1 = \kappa_2 = \kappa_3 = \kappa_4 = 0.01$, $r = 2$, $r_b = 1$, $\alpha_d = 0.001$, $\alpha_a = 0.1$, $\alpha_b = 0.01$, $V_1/V_2 = 0.1$ and $V_3/V_4 = 2$. **(E)** Effect of degree of reaction saturation on switch-like behaviour. Dependence of the steady-state levels of x_1 and y_1 on the ratio of maximum rate constants V_1/V_2 at varying levels of the Michaelis-Menten constant of the reactions 1-4. Parameter values used for plotting are $r = 2$, $r_a = r_b = 1$, $\alpha_d = 0.001$, $\alpha_a = 0.1$, $\alpha_b = 0.01$ and $V_3/V_4 = 2$; κ_1, κ_2, κ_3 , κ_4 are assumed equal and commonly denoted as κ_d.

2. Construction of an extended dynamic mathematical model for the integrated Raf-1 - MST2 pathway

2.1. Model description and assumptions

To systematically explore the emergent properties of the Raf-1 - MST2 pathway crosstalk, we developed a dynamic mathematical model that incorporated protein interactions, phosphorylation reactions and feedback loops. The kinetic scheme of this extended model is shown in Fig. 4 of the main text. The model is formulated using ordinary differential equations which are described in Tables M1-2, and the parameters are given in Supplementary Table 3. We made the following assumptions while constructing the model:

Regulation of Raf-1 kinase activity: The inhibition of MST2 does not require Raf-1 kinase activity but solely relies on the binding of Raf-1 to MST2.[1] By contrast, the activation of MEK occurs through phosphorylation of MEK and requires Raf-1 kinase activity. The regulation of Raf-1 kinase activity is a complex process.[2, 3] However, two steps are essential. Both are initiated by Raf-1 binding to activated Ras. They comprise the dephosphorylation of the inhibitory pS259 and the subsequent phosphorylation of the activating site S338. The reverse process is required for full deactivation of Raf-1. These two step transitions for Raf-1 (de)activation are described by reactions 1-4 (Fig. 4). As suggested by our data LATS1 can phosphorylate Raf-1 at S259 (reaction 2), effectively forming a negative feedback loop with a dual effect. It prevents Raf-1 from activating MEK and enhances Raf-1 binding to MST2, promoting MST2 inhibition.

MST2-Raf-1 complex formation: We assumed that only Raf-1 phosphorylated on S259, denoted pRaf-1i, can effectively bind MST2. Kinase-active Raf-1a, formed after dephosphorylation of pS259 and phosphorylation of S338, does not bind MST2, but associates with MEK instead. Our experimental data suggest that Akt-mediated phosphorylation of MST2 (pMST2i) inhibits MST2 and strongly enhances MST2 binding to pRaf-1i[4]; the K_d for the pMST2i-pRaf-1i complex (denoted pMi-pRi, reaction 5) is thus assumed to be an order of magnitude less than the K_d of MST2-pRaf-1i complex (denoted M-pRi, reaction 6).

Akt-mediated phosphorylation of MST2: We assumed that MST2 can exist in inactive or active phosphorylation states, which are induced either by Akt-mediated phosphorylation (reaction 7) or by MST2 dimerization and autophosphorylation (reaction 9), respectively. Akt inactivates MST2 by phosphorylating MST2 at two sites, T117 and T384[4], here considered as one variable (pMST2i) for simplicity. Akt-induced MST2 phosphorylation can be reversed by phosphatases (reaction 8). Importantly, pMST2i effectively binds pRaf-1i but not RASSF1A. As the formation of MST2-RASSF1A and MST2-pRaf-1i complexes is mutually exclusive,

© 2014 Macmillan Publishers Limited. All rights reserved.

and the binding of pMST2i to RASSF1A is very weak[4], the formation of a pMST2i - RASSF1A complex is not considered in our model.

MST2 activation is facilitated by RASSF1A: Active MST2 (MST2a) is generated through dimerization of two inactive MST2 molecules followed by autophosphorylation[1, 5, 6] (reaction 9). Although it is conceivable that an active MST2 molecule can dimerize with an inactive MST2 molecule, this possibility is not considered in the model due to the lack of supporting experimental evidence. Another assumption is that MST2 dimers exist only transiently, and then give rise to monomer forms of active MST2 following autophosphorylation. This assumption is based on the observation that MST2 dimerization as well as the interaction of MST2 with RASSF1A is mediated by the SARAH domain[7, 8], and structural studies which show that SARAH domain interactions are binary with no evidence of ternary complexes, such as a MST dimer interacting with a RASSF1A protein.[7] Experimental data show that RASSF1A enhances the activation of MST2 in cells.[4, 9-12] The mechanism of this activation is not fully understood, but recent evidence[13] suggests that RASSF1A binding protects active MST2a against dephosphorylation of the activating residues by phosphatases such as PP2A (reaction 10). Therefore, MST2a becomes enriched in the complex with RASSF1A, and we estimated that the K_d for the MST2a-RASSF1A complex formation (denoted Ma-F1A, reaction 11) is an order of magnitude less than the K_d of the MST2-RASSF1A complex (denoted M-F1A, reaction 12). Furthermore, we assumed MST2 can be activated while in complex with RASSF1A (reaction 13). Thus, MST2 can signal to the downstream components of the pathway either as activated monomer or when associated with RASSF1A (reaction 14).

LATS1 activation and negative feedback loop: LATS1 is a direct substrate of active MST2[9-11, 14]. We assumed that active MST2 phosphorylates LATS1 equally well regardless whether MST2 is free or bound to RASSF1A (reaction 14). As shown in Fig. 3, activated LATS1 can phosphorylate Raf-1 at S259 (reaction 2), thereby forming a negative feedback loop.

ERK activation following activation of Raf-1: Consistent with previous data[15-17] we assumed that only Raf-1 phosphorylated at S338 (active Raf-1a) can bind and activate MEK, which subsequently activates ERK. We modelled this cascade as previously described[18, 19], including the double (de)phosphorylation cycles of MEK and ERK (reactions 16-23). We also incorporated the negative feedback from ERK to Raf-1, whereby ERK phosphorylates Raf-1 resulting in the inhibition of Ras binding and kinase activity (reaction 3).[18, 20]

2.2. Modelling different signalling inputs for different experimental setups.

Similarly to the core model (Fig. M2), we first used Michaelis-Menten descriptions of enzyme reactions to model the (de)phosphorylation events. Since our primary interest is the steady-state behaviour of the system, a Michaelis-Menten description is relevant and sufficient for this purpose. Nevertheless, for completeness we also constructed a detailed elementary-step model of the system (Section 3) where all the enzymatic reactions are described using mass-action kinetic law and confirmed the salient predictions with this model.

To accommodate different experimental setups, the Raf-1/MST2 kinetic model described above can use RasGTP and active Akt or serum growth factors as inputs. For steady-state simulations taking RasGTP or active Akt as input, the responses of relevant molecular species such as active Raf-1 (Raf-1a) or MST2 (MST2a) to increasing input levels can readily

© 2014 Macmillan Publishers Limited. All rights reserved.

be produced using the reaction rates and differential equations given in Tables M1-2. When serum is considered as model input, the rates of reactions 1 and 7 are modified (Fig. 4), since steady-state levels of active Ras and Akt become functions of serum level, as follows (see Supplementary Table 1):

$$v_1 = \frac{k_1 \cdot \text{RasGTP(Serum)} \cdot \text{pRaf-1i}}{K_{m1} + \text{pRaf-1i}}$$

$$v_7 = \frac{k_7 \cdot \text{Akt(Serum)} \cdot \text{MST2} \cdot (1+k_{act} \cdot \text{RasGTP})}{K_{m7} + \text{MST2}},$$

where RasGTP(Serum) and Akt(Serum) are functions of the level of serum. Assuming a linear relationship (for the non-saturating concentration range), we approximate the inputs to the Raf1/MST2 pathways, which are serum-dependent activated Ras and Akt, as follows,

$$\text{RasGTP(Serum)} = \text{RasGTP}_0 \cdot (1+k_{sr1} \cdot \text{Serum})$$

$$\text{Akt(Serum)} = \text{Akt}_0 \cdot (1+k_{sr2} \cdot \text{Serum}).$$

RasGTP_0 and Akt_0 are the basal levels of RasGTP and active Akt (unstimulated). The parameters k_{sr1} and k_{sr2} relate the serum levels to the steady state levels of RasGTP and active Akt, respectively.

2.3. Model calibration and parameter selection

As many of the kinetic parameters in the Raf-1/MST2 system are unknown at the present time, we explored wide ranges of parameter space to understand the dynamical properties of the system. Since the prime purpose of computational modelling is to provide the basis for guiding experimental analysis and testing explicit hypotheses; a model by itself is not an objective "truth," but it can be used to falsify or confirm a specific hypothesis. Detailed, systematic parameter exploration compatible with experimentally observed behaviour therefore constitutes an appropriate approach to tackle the lack of measured parameters.

Knowledge of the rate constants of the forward and backward reactions was required to describe the dynamic behaviour of the system. In our model, these rates were restricted to be within the typical ranges for protein-protein interactions. For example, the association of protein molecules into dimers or larger complexes occurs with typical rate constants of the order of 10^{-4} to 10^{-1} nM^{-1} s^{-1}.[21-23] In addition, the reaction rates were always constrained to be not faster than the diffusion limit. Moreover, experimental data suggested large differences in the equilibrium constant K_d for specific reactions in the system. We therefore selected the corresponding association and dissociation rates to be in accordance with the differential K_d values (see Section 2.1 and Tables M3, M6). Strikingly, in all these wide ranges of parameter choice, switches could be observed for functionally relevant proteins, such as active phosphorylated form of Raf-1 and active MST2.

As shown in section 1.2, the existence of the switches critically depends on the "core module" which governs the binding crosstalk between MST2 and Raf-1. Our analysis showed that the switching behaviours predicted by our model persists as long as the "core reactions" are under saturating condition, even when the kinetic rates of the peripheral reactions are widely varied. Then, to obtain an optimal parameter set used for simulations plotting, we manually fitted the model using a training set data measured experimentally for transient RasGTP and active Akt (see section 2.4). The objective of this fitting was that time-

© 2014 Macmillan Publishers Limited. All rights reserved.

dependent transient RasGTP and active Akt inputs would generate transient active ERK profiles that were observed experimentally (Fig. 1B). The fitted parameter values presented in Supplementary Table 3 were in agreement with the experimental observations for similar reaction types. Moreover, although the parameter values following the above fitting procedure cannot be uniquely identified, the simulated behaviour had a predictive power as confirmed by independent validation experiments.

2.4. Parameter fitting using temporal dynamics data

Our experimental data showed that Ras activation followed transient kinetics, while active phosphorylated Akt showed saturation kinetics upon serum stimulation (Fig.M3). Therefore, to model temporal dynamics in response to serum stimulation we used active Akt and RasGTP as time-dependent input functions estimated from the data. The estimation procedure for the RasGTP function is given elsewhere[24], and Akt is described by a simple saturating function of time. The corresponding fitting equations have the following form:

$$RasGTP(t) = 2 + \alpha(\beta - 285e^{-t/192} \quad 254e^{-t/1260})$$

$$Akt(t) = \alpha_1 + \frac{\beta_1 * t}{1000 + t}$$

Fig. M3 shows that these functions fit the data within a two hour timeframe, assuming that the peak of Ras activation corresponds to about 50nM RasGTP, and Akt activation peaks at 100nM active Akt. By changing the parameters α, β, α_1, β_1 the magnitudes and peaks of the RasGTP and Akt input funtions can be varied while keeping similar time-dependent patterns.

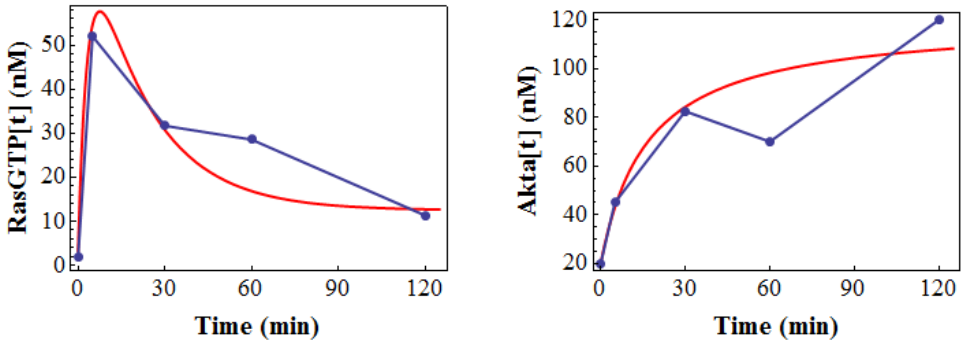

Fig. M3. Input functions RasGTP and active Akt estimated from experimental data. The red lines are the estimated continuous functions. Blue lines and dots represent quantified experimental data. Parameter values are the following, $\alpha = 0.3, \beta = 35, \alpha_1 = 20, \beta_1 = 100$.

Replacing the fixed RasGTP and Akt variables in Supplementary Table 1 by the time-dependent functions of RasGTP and Akt estimated above, we integrated the resulting ODE system and fitted the parameters to the transient temporal dynamics of phosphorylated ERK, MEK and active MST2 measured experimentally (Fig. 1b). For illustration, the model simulations for the time-course dynamics of the active MST2 (MST2a) and ERK (ppERK) levels are shown in Fig. M4 as examples. The obtained best fit set of parameter is presented in Supplementary Table 3, and used to simulate steady-state responses of the system.

© 2014 Macmillan Publishers Limited. All rights reserved.

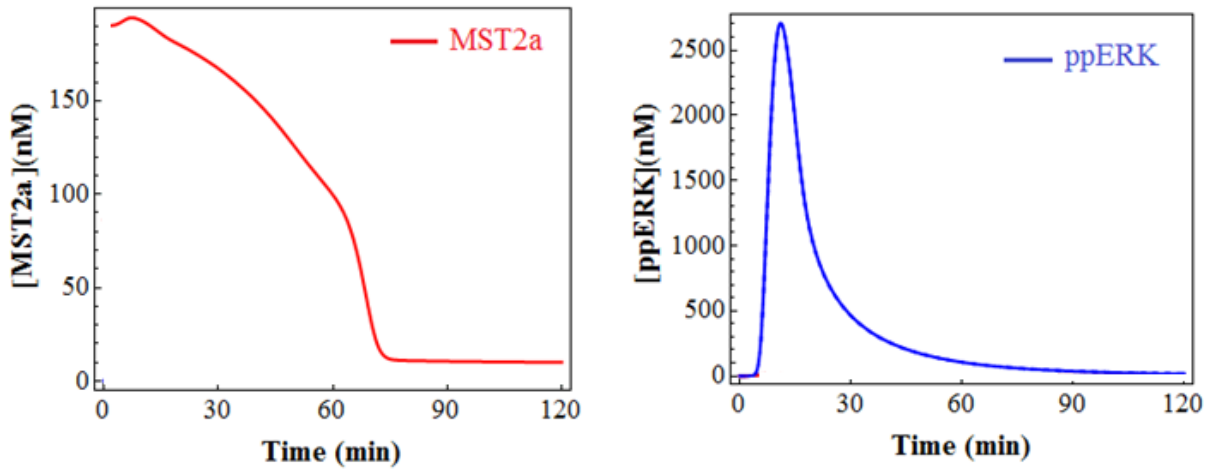

Fig. M4. Temporal response of active MST2 and ERK simulated by the Raf-1/MST2 model using the input functions RasGTP and active Akt given in Fig.M3. The remaining parameter values used for plotting are given in Supplementary Table 3.

Supplementary Table 1. Reactions and reaction rates of the Raf-1/MST2 kinetic model

	Reactions	**Reaction rates**
v_1 (*)	pRaf-1i → Raf-1	$\frac{k_1 \cdot \text{RasGTP} \cdot \text{pRaf-1i}}{K_{m1} + \text{pRaf-1i}}$
v_2	Raf-1 → pRaf-1i	$\frac{k_{2a} \cdot \text{LATS1a} \cdot \text{Raf-1}}{K_{m2a} + \text{Raf-1}} + \frac{k_{2b} \cdot \text{Kin} \cdot \text{Raf-1}}{K_{m2b} + \text{Raf-1}}$
v_3	Raf-1 → Raf-1a	$\frac{V_3 \cdot \text{Raf-1}}{K_{m3} + \text{Raf-1}} \cdot \left(\frac{1 + Fa \cdot (\text{ppERK/Ka})}{1 + (\text{ppERK/Ka})} \right)$
v_4	Raf-1a → Raf-1	$\frac{V_4 \cdot \text{Raf-1a}}{K_{m4} + \text{Raf-1a}}$
v_5	pMST2i + pRaf-1i ↔ pMi-pRi	$k_{5f} \cdot \text{pMST2i} \cdot \text{pRaf-1i} - k_{5r} \cdot \text{pMi-pRi}$
v_6	MST2 + pRaf-1i ↔M-pRi	$k_{6f} \cdot \text{MST2} \cdot \text{pRaf-1i} - k_{6r} \cdot \text{M-pRi}$
v_7 (*)	MST2 → pMST2i	$\frac{k_7 \cdot \text{Akt} \cdot \text{MST2} \cdot (1 + k_{act} \cdot \text{RasGTP})}{K_{m7} + \text{MST2}}$
v_8	pMST2i → MST2	$\frac{k_8 \cdot \text{PP2A} \cdot \text{pMST2i}}{K_{m8} + \text{pMST2i}}$
v_9	MST2 + MST2 → 2 MST2a	$k_9 \cdot \text{MST2} \cdot \text{MST2}$
v_{10}	MST2a → MST2	$\frac{k_{10} \cdot \text{PP2A} \cdot \text{MST2a}}{K_{m10} + \text{MST2a}}$
v_{11}	MST2a + RASSF1A ↔ Ma-F1A	$k_{11f} \cdot \text{MST2a} \cdot \text{RASSF1A} - k_{11r} \cdot \text{Ma-F1A}$
v_{12}	MST2 + RASSF1A ↔ M-F1A	$k_{12f} \cdot \text{MST2} \cdot \text{RASSF1A} - k_{12r} \cdot \text{M-F1A}$

© 2014 Macmillan Publishers Limited. All rights reserved.

v_{13}	M-F1A → Ma-F1A	$\frac{V_{13} \cdot \text{M-F1A}}{K_{m13} + \text{M-F1A}}$
v_{14}	LATS1 → LATS1a	$\frac{k_{14a} \cdot \text{MST2a} \cdot \text{LATS1}}{K_{m14a} + \text{LATS1}} + \frac{k_{14b} \cdot \text{Ma-F1A} \cdot \text{LATS1}}{K_{m14b} + \text{LATS1}}$
v_{15}	LATS1a → LATS1	$\frac{V_{15} \cdot \text{LATS1a}}{K_{m15} + \text{LATS1a}}$
v_{16a}	Raf-1a + MEK ↔ Ra-Mk	$k_{16af} \cdot \text{Raf-1a} \cdot \text{MEK} - k_{16ar} \cdot \text{Ra-Mk}$
v_{16b}	Ra-Mk → pMEK + Raf-1a	$k_{16b} \cdot \text{Ra-Mk}$
v_{17}	pMEK → MEK	$\frac{V_{17} \cdot \text{pMEK}}{K_{m17} + \text{pMEK} + \text{ppMEK} \cdot (K_{m17}/K_{m19})}$
v_{18a}	Raf-1a + pMEK ↔ Ra-pMk	$k_{18af} \cdot \text{Raf-1a} \cdot \text{pMEK} - k_{18ar} \cdot \text{Ra-pMk}$
v_{18b}	Ra-pMk → ppMEK + Raf-1a	$k_{18b} \cdot \text{Ra-pMk}$
v_{19}	ppMEK → pMEK	$\frac{V_{19} \cdot \text{ppMEK}}{K_{m19} + \text{ppMEK} + \text{pMEK} \cdot (K_{m19}/K_{m17})}$
v_{20}	ERK → pERK	$\frac{k_{20} \cdot \text{ppMEK} \cdot \text{ERK}}{K_{m20} + \text{ERK} + \text{pERK} \cdot (K_{m20}/K_{m22})}$
v_{21}	pERK → ERK	$\frac{V_{21} \cdot \text{pERK}}{K_{m21} + \text{pERK} + \text{ppERK} \cdot (K_{m21}/K_{m23}) + \text{ERK} \cdot (K_{m21}/\text{Ki})}$
v_{22}	pERK → ppERK	$\frac{k_{22} \cdot \text{ppMEK} \cdot \text{pERK}}{K_{m22} + \text{pERK} + \text{ERK} \cdot (K_{m22}/K_{m20})}$
v_{23}	ppERK → pERK	$\frac{V_{23} \cdot \text{ppERK}}{K_{m23} + \text{ppERK} + \text{pERK} \cdot (K_{m23}/K_{m21}) + \text{ERK} \cdot (K_{m23}/\text{Ki})}$

(*) Note that when considering serum as input, the reactions rates v_1 and v_7 are modified (see above text for more details).

© 2014 Macmillan Publishers Limited. All rights reserved.

Supplementary Table 2. Ordinary differential equations of the Raf-1/MST2 kinetic model. The reaction rates are given in Supplementary Table 1.

Left-hand Sides	**Right-hand Sides**	**Initial Concentrations (nM)**	**Comments**
d[pRaf1i]/dt	$-v_1 + v_2 - v_5 - v_6$	750	Measured in this study
d[Raf1a]/dt	$v_3 - v_4 - v_{16a} + v_{16b} - v_{18a} + v_{18b}$	0	
d[Raf1]/dt	$v_1 - v_2 - v_3 + v_4$	0	
d[pMST2i]/dt	$-v_5 + v_7 - v_8$	0	
d[MST2]/dt	$-v_6 - v_7 + v_8 - 2v_9 + v_{10} - v_{12}$	1500	Measured in this study
d[MST2a]/dt	$2v_9 - v_{10} - v_{11}$	0	
d[Ma-F1A]/dt	$v_{11} + v_{13}$	0	
d[M-F1A]/dt	$v_{12} - v_{13}$	0	
d[RASSF1A]/dt	$-v_{11} - v_{12}$	100	0 nM was used to simulate the absence of RASSF1A, 500 nM was used for high RASSF1A level
d[LATS1]/dt	$-v_{14} + v_{15}$	100	Estimated
d[LATS1a]/dt	$v_{14} - v_{15}$	0	
d[MEK]/dt	$-v_{16a} + v_{17}$	1600	Measured in this study
d[pMEK]/dt	$v_{16b} - v_{17} - v_{18a} + v_{19}$	0	
d[ppMEK]/dt	$v_{18b} - v_{19}$	0	
d[ERK]/dt	$-v_{20} + v_{21}$	3000	Measured in this study
d[pERK]/dt	$v_{20} - v_{21} - v_{22} + v_{23}$	0	
d[ppERK]/dt	$v_{22} - v_{23}$	0	
d[pMi-pRi]/dt	v_5	0	
d[M-pRi]/dt	v_6	0	
d[Ra-Mk]/dt	$v_{16a} - v_{16b}$	0	
d[Ra-pMk]/dt	$v_{18a} - v_{18b}$	0	

© 2014 Macmillan Publishers Limited. All rights reserved.

Supplementary Table 3. Parameter values used in the model. Concentrations and the Michaelis-Menten constants (K_ms) are given in nM. First- and second-order rate constants are expressed in s^{-1} and nM^{-1} s^{-1}. Maximum rates Vs are expressed in nM s^{-1}.

Parameters	**Comments and references**
k_1=0.02, K_{m1} = 1	Estimated
k_{2a} = 0.01, K_{m2a} =1, k_{2b} = 0.01, K_{m2b} = 1, Kin = 20	Estimated
V_3 = 2, K_{m3} = 1, Ka = 1000, Fa= 0.5	Estimated
V_4 = 1, K_{m4} = 1	Estimated
k_{5f} = 0.01, k_{5r} = 0.1	Assuming K_d of reaction 5 is an order of magnitude less than that of reaction 6.
k_{6f} = 0.001, k_{6r} = 0.1	Estimated
k_7 = 0.008, K_{m7} = 1	Estimated
k_8 = 0.01, K_{m8} = 1, PP2A = 50	Estimated
k_9 = 0.00035	Estimated
k_{10} = 10, K_{m10} = 50	Estimated
k_{11f} = 0.01, k_{11r} = 0.1	Assuming K_d of reaction 11 is an order of magnitude less than that of reaction 12.
k_{12f} = 0.01, k_{12r} = 1	Estimated
V_{13} = 10, K_{m13} = 50	Estimated
k_{14a} = 0.05, K_{m14a} = 50, k_{14b} = 0.05, K_{m14b} = 50	Estimated
V_{15} = 0.05, K_{m15} = 50	Estimated
k_{16af} = 0.01, k_{16ar} = 1, k_{16b} = 5	Estimated
V_{17} = 250, K_{m17} = 400	Estimated
k_{18af} = 0.01, k_{18ar} = 1, k_{18b} = 5	Estimated
V_{19} = 250, K_{m19} = 400	Estimated
k_{20} = 1, K_{m20} = 500	Estimated
V_{21} = 100, K_{m21}= 500, Ki =1	Estimated
k_{22} = 10, K_{m22} = 500	Estimated
V_{23} = 100, K_{m23}= 100	Estimated

© 2014 Macmillan Publishers Limited. All rights reserved.

3. Development and analysis of an elementary-step kinetic model

The model described in previous sections utilised Michaelis-Menten law of kinetics to describe most of the enzymatic reactions (e.g. (de)phosphorylation). A salient result of our modelling and experimental work is that competing protein interactions play an important role in signal coordination between the MST2 and ERK pathways. Therefore, we deemed it important to also develop an elementary-step model that accounts for explicit associations and dissociations between the proteins involved in the key reactions. As we show below, this detailed elementary step model also can exhibit switch-like behaviours as observed in the non-elementary model.

3.1. Development of the elementary step model

Figure M3 shows the kinetic scheme of the elementary-step model. Compared to the non-elementary step model shown in Fig. 4, the phosphorylation of MST2 by Akt (reaction 7), activation of Raf-1 by RasGTP (reaction 1) and the whole module of ERK activation cascade (reactions 16-23) as well as the ppERK to Raf-1 negative feedback are now explicitly modelled with mass-action kinetics (reactions 1a, 7a, 16a-23a for the enzyme-substrate binding, and reactions 1b, 7b, 16b-23b for the catalytic conversion, Fig. M5). Consequently, the elementary-step model includes new variables which are the enzyme-substrate complexes for these reactions (see the legend to Fig. M5 for details). Since the negative feedback from active ERK (ppERK) to Raf-1 is caused by direct phosphorylation of Raf-1 by ERK, which inhibits the activation of Raf-1 by RasGTP[18, 20], we modelled this feedback with two sets of mass-action reactions 24-26 and 27-29 (Fig. M5). The model's reaction rates, differential equations and parameter values are given in Tables M4-M6.

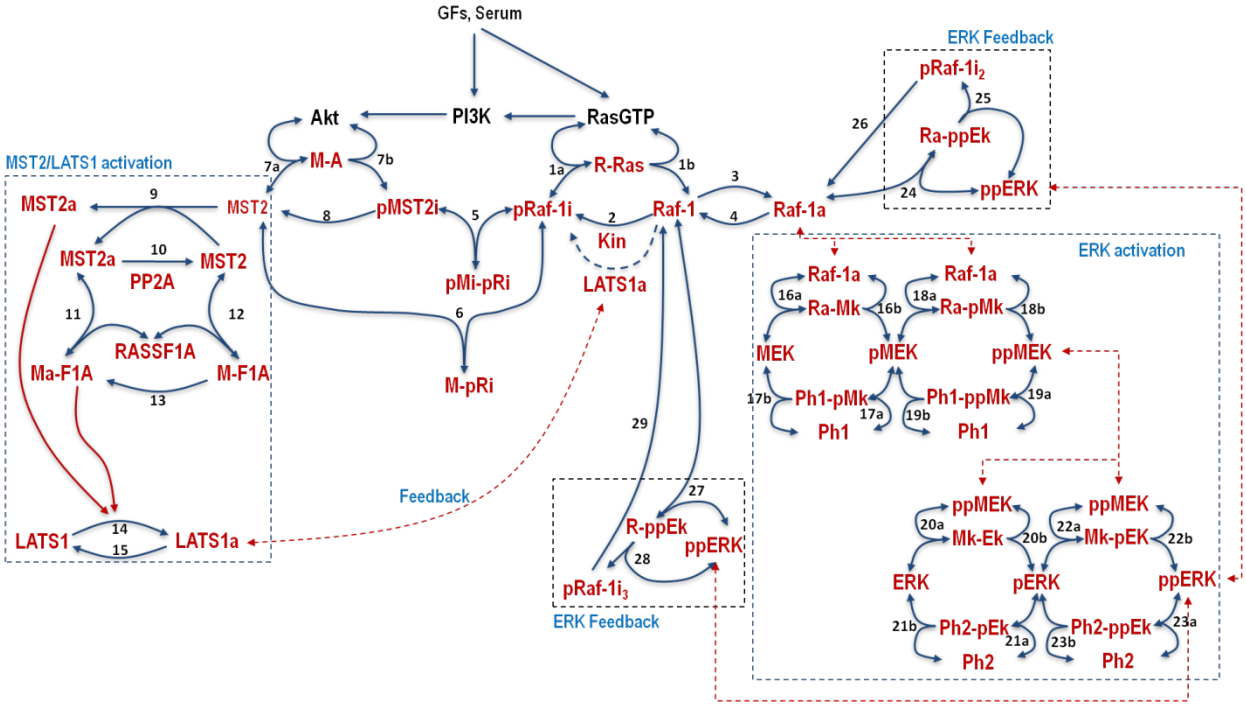

Fig. M5. Kinetic scheme of the elementary-step reaction model of the Raf-1/MST2 system. The nomenclature of molecular species is the same as for the reduced model above that used the Michaelis-Menten kinetics. For the additional species, M-A = MST2 and Akt complex; R-Ras = Raf-1 and RasGTP complex; Ra-Mk = Raf-1a and MEK complex; Ra-pMk = Raf-1a and pMEK complex; Ph1 = phosphatase which dephosphorylates

© 2014 Macmillan Publishers Limited. All rights reserved.

phosphorylated MEK; Ph1-pMk = Ph1 and pMEK complex; Ph1-ppMk = Ph1 and ppMEK complex; Mk-Ek = ppMEK and ERK complex, Mk-pEk = ppMEK and pERK complex; Ph2 = phosphatase which dephosphorylates phosphorylated ERK; Ph2-pEk = Ph2 and pERK complex; Ph2-ppEk = Ph2 and ppERK complex; Ra-ppEk and R-ppEK = complex of Raf-1a, Raf-1 and ppERK, pRaf-1i_2 and pRaf-1i_3 are inactive forms of Raf-1 resulting from phosphorylation of Raf-1a and Raf-1 by ppERK.

Supplementary Table 4. Reactions and reaction rates of the elementary-step Raf-1/MST2 kinetic model

	Reactions	**Reaction rates**
v_{1a}	pRaf-1i → Raf-1	$k_{1af} \cdot \text{RasGTP} \cdot \text{pRaf-1i} - k_{1ar} \cdot \text{R-Ras}$
v_{1b}	R-Ras → Raf-1 + RasGTP	$k_{1b} \cdot \text{R-Ras}$
v_2	Raf-1 → pRaf-1i	$\frac{k_{2a} \cdot \text{LATS1a} \cdot \text{Raf-1}}{K_{m2a} + \text{Raf-1}} + \frac{k_{2b} \cdot \text{Kin} \cdot \text{Raf-1}}{K_{m2b} + \text{Raf-1}}$
v_3	Raf-1 + RasGTP ↔ R-Ras	$\frac{V_3 \cdot \text{Raf-1}}{K_{m3} + \text{Raf-1}}$
v_4	Raf-1a → Raf-1	$\frac{V_4 \cdot \text{Raf-1a}}{K_{m4} + \text{Raf-1a}}$
v_5	pMST2i + pRaf-1i ↔ pMi-pRi	$k_{5f} \cdot \text{pMST2i} \cdot \text{pRaf-1i} - k_{5r} \cdot \text{pMi-pRi}$
v_6	MST2 + pRaf-1i ↔M-pRi	$k_{6f} \cdot \text{MST2} \cdot \text{pRaf-1i} - k_{6r} \cdot \text{M-pRi}$
v_{7a}	MST2 + Akt ↔ M-A	$k_{7af} \cdot \text{MST2} \cdot \text{Akt} \cdot (1 + k_{act} \cdot \text{RasGTP}) - k_{7ar} \cdot \text{M-A}$
v_{7b}	M-A → pMST2i + Akt	$k_{7b} \cdot \text{M-A}$
v_8	pMST2i → MST2	$\frac{k_8 \cdot \text{PP2A} \cdot \text{pMST2i}}{K_{m8} + \text{pMST2i}}$
v_9	MST2 + MST2 → 2 MST2a	$k_9 \cdot \text{MST2} \cdot \text{MST2}$
v_{10}	MST2a → MST2	$\frac{k_{10} \cdot \text{PP2A} \cdot \text{MST2a}}{K_{m10} + \text{MST2a}}$
v_{11}	MST2a + RASSF1A ↔ Ma-F1A	$k_{11f} \cdot \text{MST2a} \cdot \text{RASSF1A} - k_{11r} \cdot \text{Ma-F1A}$
v_{12}	MST2 + RASSF1A ↔ M-F1A	$k_{12f} \cdot \text{MST2} \cdot \text{RASSF1A} - k_{12r} \cdot \text{M-F1A}$
v_{13}	M-F1A → Ma-F1A	$\frac{V_{13} \cdot \text{M-F1A}}{K_{m13} + \text{M-F1A}}$
v_{14}	LATS1 → LATS1a	$\frac{k_{14a} \cdot \text{MST2a} \cdot \text{LATS1}}{K_{m14a} + \text{LATS1}} + \frac{k_{14b} \cdot \text{Ma-F1A} \cdot \text{LATS1}}{K_{m14b} + \text{LATS1}}$
v_{15}	LATS1a → LATS1	$\frac{V_{15} \cdot \text{LATS1a}}{K_{m15} + \text{LATS1a}}$
v_{16a}	Raf-1a + MEK ↔ Ra-Mk	$k_{16af} \cdot \text{Raf-1a} \cdot \text{MEK} - k_{16ar} \cdot \text{Ra-Mk}$
v_{16b}	Ra-Mk → pMEK + Raf-1a	$k_{16b} \cdot \text{Ra-Mk}$
v_{17a}	Ph1 + pMEK ↔ Ph1-pMk	$k_{17af} \cdot \text{Ph1} \cdot \text{pMEK} - k_{17ar} \cdot \text{Ph1-pMk}$

© 2014 Macmillan Publishers Limited. All rights reserved.

v_{17b}	Ph1-pMk → Ph1 + MEK	$k_{17b} \cdot \text{Ph1-pMk}$
v_{18a}	Raf-1a + pMEK ↔ Ra-pMk	$k_{18af} \cdot \text{Raf-1a} \cdot \text{pMEK} - k_{18ar} \cdot \text{Ra-pMk}$
v_{18b}	Ra-pMk → ppMEK + Raf-1a	$k_{18b} \cdot \text{Ra-pMk}$
v_{19a}	Ph1 + ppMEK ↔ Ph1-ppMk	$k_{19af} \cdot \text{Ph1} \cdot \text{ppMEK} - k_{19ar} \cdot \text{Ph1-ppMk}$
v_{19b}	Ph1-ppMk → Ph1 + pMEK	$k_{19b} \cdot \text{Ph1-ppMk}$
v_{20a}	ppMEK + ERK ↔ Mk-Ek	$k_{20af} \cdot \text{ppMEK} \cdot \text{ERK} - k_{20ar} \cdot \text{Mk-Ek}$
v_{20b}	Mk-Ek → pERK + ppMEK	$k_{20b} \cdot \text{Mk-Ek}$
v_{21a}	Ph2 + pERK ↔ Ph2-pEk	$k_{21af} \cdot \text{Ph2} \cdot \text{pERK} - k_{21ar} \cdot \text{Ph2-pEk}$
v_{21b}	Ph2-pEk → Ph2 + ERK	$k_{21b} \cdot \text{Ph2-pEk}$
v_{22a}	ppMEK + pERK ↔ Mk-pEk	$k_{22af} \cdot \text{ppMEK} \cdot \text{pERK} - k_{22ar} \cdot \text{Mk-pEk}$
v_{22b}	Mk-pEk → ppERK + ppMEK	$k_{22b} \cdot \text{Mk-Ek}$
v_{23a}	Ph2 + ppERK ↔ Ph2-ppEk	$k_{23af} \cdot \text{Ph2} \cdot \text{ppERK} - k_{23ar} \cdot \text{Ph2-ppEk}$
v_{23b}	Ph2-ppEk → Ph2 + pERK	$k_{23b} \cdot \text{Ph2-ppEk}$
v_{24}	Raf-1a + ppERK ↔ Ra-ppEk	$k_{24f} \cdot \text{Raf-1a} \cdot \text{ppERK} - k_{24r} \cdot \text{Ra-ppEk}$
v_{25}	Ra-ppEk → ppERK + $pRaf\text{-}1i_2$	$k_{25} \cdot \text{Ra-ppEk}$
v_{26}	$pRaf\text{-}1i_2$ → Raf-1a	$\frac{V_{26} \cdot pRaf\text{-}1i_2}{K_{m26} + pRaf\text{-}1i_2}$
v_{27}	Raf-1 + ppERK ↔ R-ppEk	$k_{27f} \cdot \text{Raf-1} \cdot \text{ppERK} - k_{27r} \cdot \text{R-ppEk}$
v_{28}	R-ppEk → ppERK + $pRaf\text{-}1i_3$	$k_{28} \cdot \text{R-ppEk}$
v_{29}	$pRaf\text{-}1i_3$ → Raf-1	$\frac{V_{29} \cdot pRaf\text{-}1i_3}{K_{m29} + pRaf\text{-}1i_3}$

Supplementary Table 5. Ordinary differential equations of the elementary-step Raf-1/MST2 kinetic model. The reaction rates are given in Supplementary Table 4.

Left-hand Sides	Right-hand Sides	Initial Concentrations (nM)	Comments
d[pRaf1i]/dt	$-v_{1a} + v_2 - v_5 - v_6$	750	Measured in this study
d[Raf1a]/dt	$v_3 - v_4 - v_{16a} + v_{16b} - v_{18a} + v_{18b} - v_{24} + v_{26}$	0	
d[Raf1]/dt	$v_{1b} - v_2 - v_3 + v_4 - v_{27} + v_{29}$	0	
d[pMST2i]/dt	$-v_5 + v_7 - v_8$	0	
d[MST2]/dt	$-v_6 - v_7 + v_8 - 2v_9 + v_{10} - v_{12}$	1500	Measured in this study
d[MST2a]/dt	$2v_9 - v_{10} - v_{11}$	0	
d[Ma-F1A]/dt	$v_{11} + v_{13}$	0	
d[M-F1A]/dt	$v_{12} - v_{13}$	0	
d[RASSF1A]/dt	$-v_{11} - v_{12}$	100	0 nM was used to simulate the absence of

© 2014 Macmillan Publishers Limited. All rights reserved.

			RASSF1A, 500 nM was used for high RASSF1A level
d[LATS1]/dt	$-v_{14} + v_{15}$	100	Estimated
d[LATS1a]/dt	$v_{14} - v_{15}$	0	
d[MEK]/dt	$-v_{16a} + v_{17b}$	1600	Measured in this study
d[pMEK]/dt	$v_{16b} - v_{17a} - v_{18a} + v_{19b}$	0	
d[ppMEK]/dt	$v_{18b} - v_{19a}$	0	
d[ERK]/dt	$-v_{20a} + v_{21b}$	3000	Measured in this study
d[pERK]/dt	$v_{20b} - v_{21a} - v_{22a} + v_{23b}$	0	
d[ppERK]/dt	$v_{22b} - v_{23a} - v_{24} + v_{25} - v_{27} + v_{28}$	0	
d[Ra-Mk]/dt	$v_{16a} - v_{16b}$	0	
d[Ra-pMk]/dt	$v_{18a} - v_{18b}$	0	
d[Ph1-pMk]/dt	$v_{17a} - v_{17b}$	0	
d[Ph1-ppMk]/dt	$v_{19a} - v_{19b}$	0	
d[Ph1]/dt	$v_{17b} - v_{17a} + v_{19b} - v_{19a}$	100	Estimated
d[Mk-Ek]/dt	$v_{20a} - v_{20b}$	0	
d[Mk-pEk]/dt	$v_{22a} - v_{22b}$	0	
d[Ph2-pEk]/dt	$v_{21a} - v_{21b}$	0	
d[Ph2-ppEk]/dt	$v_{23a} - v_{23b}$	0	
d[Ph2]/dt	$v_{21b} - v_{21a} + v_{23b} - v_{23a}$	100	Estimated
d[pMi-pRi]/dt	v_5	0	
d[M-pRi]/dt	v_6	0	
d[RasGTP]/dt	$v_{1b} - v_{1a}$	varying	
d[R-Ras]/dt	$v_{1a} - v_{1b}$	0	
d[Akt]/dt	$v_{7b} - v_{7a}$	20	
d[M-A]/dt	$v_{7a} - v_{7b}$	0	
d[Ra-ppEk]/dt	$v_{24} - v_{25}$	0	
d[pRaf-1i_2]/dt	$v_{25} - v_{26}$	0	
d[R-ppEk]/dt	$v_{27} - v_{28}$	0	
d[pRaf-1i_3]/dt	$v_{28} - v_{29}$	0	

© 2014 Macmillan Publishers Limited. All rights reserved.

Supplementary Table 6. Parameter values used in the elementary-step Raf-1/MST2 kinetic model

Concentrations and the Michaelis-Menten constants (K_ms) are given in nM. First- and second-order rate constants are expressed in s^{-1} and nM^{-1} s^{-1}. Maximum rates Vs are expressed in nM s^{-1}.

Parameters	**Comments and references**
k_{1af} , k_{1ar} , k_{1b}	Varying (see Fig. M5)
k_{2a} = 0.01, K_{m2a} =1, k_{2b} = 0.01, K_{m2b} = 1, Kin = 20	Estimated
V_3=1, K_{m3} = 1	Estimated
V_4 = 1, K_{m4} = 1	Estimated
k_{5f} = 0.01, k_{5r} = 0.1	Assuming K_d of reaction 5 is an order of magnitude less than that of reaction 6.
k_{6f} = 0.001, k_{6r} = 0.1	Estimated
k_{7af}, k_{7ar} , k_{7b}	Varying (see Fig. M5)
k_8 = 0.01, K_{m8} = 1, PP2A = 50	Estimated
k_9 = 0.00035	Estimated
k_{10} = 10, K_{m10} = 50	Estimated
k_{11f} = 0.01, k_{11r} = 0.1	Assuming that the K_d of reaction 11 is an order of magnitude less than the K_d of reaction 12.
k_{12f} = 0.01, k_{12r} = 1	Estimated
V_{13} = 10, K_{m13} = 50	Estimated
k_{14a} = 0.05, K_{m14a} = 50, k_{14b} = 0.05, K_{m14b} = 50	Estimated
V_{15} = 0.05, K_{m15} = 50	Estimated
k_{16af} = 0.049, k_{16ar} = 0.033, k_{16b} = 3.5	[18, 25]
k_{17af} = 0.001, k_{17ar} = 0.5, k_{17b} = 0.058	[18, 25]
k_{18af} = 0.049, k_{18ar} = 0.033, k_{18b} = 2.9	[18, 25]
k_{19af} = 0.06, k_{19ar} = 0.8, k_{19b} = 0.058	[18, 25]
k_{20af} = 0.223, k_{20ar} = 0.018, k_{20b} = 16	[18, 25]
k_{21af} = 0.021, k_{21ar} = 0.5, k_{21b} = 0.246	[18, 25]
k_{22af} = 0.223, k_{22ar} = 0.018, k_{22b} = 5.7	[18, 25]
k_{23af} = 0.059, k_{23ar} = 0.6, k_{23b} = 0.246	[18, 25]
k_{24af} = 0.003 , k_{24ar} = 0.1, k_{24b} = 1, V_{26} = 100 , K_{m26} = 50	[18, 25]
k_{27af} = 0.003, k_{27ar} = 0.1 , k_{27b} = 1, V_{29} = 100 , K_{m29} = 50	[18, 25]
Akt = 20	Estimated

© 2014 Macmillan Publishers Limited. All rights reserved.

3.2. Simulations of the elementary-step model

To evaluate whether the elementary-step model is also capable of generating steep switch-like responses for both the MST2 and Raf-1 pathways, we simulated responses of active MST2a and Raf-1a to increasing levels of RasGTP. Our simulations (Fig. M6) show that under appropriate conditions using reasonable elementary parameter values, the elementary-step model exhibits steep ON and OFF switching behaviour for active MST2 and ON switches for active Raf-1 under different conditions, similar to the behaviour demonstrated for the model that used the Michaelis-Menten type rate equations (Fig. 5a in the main text).

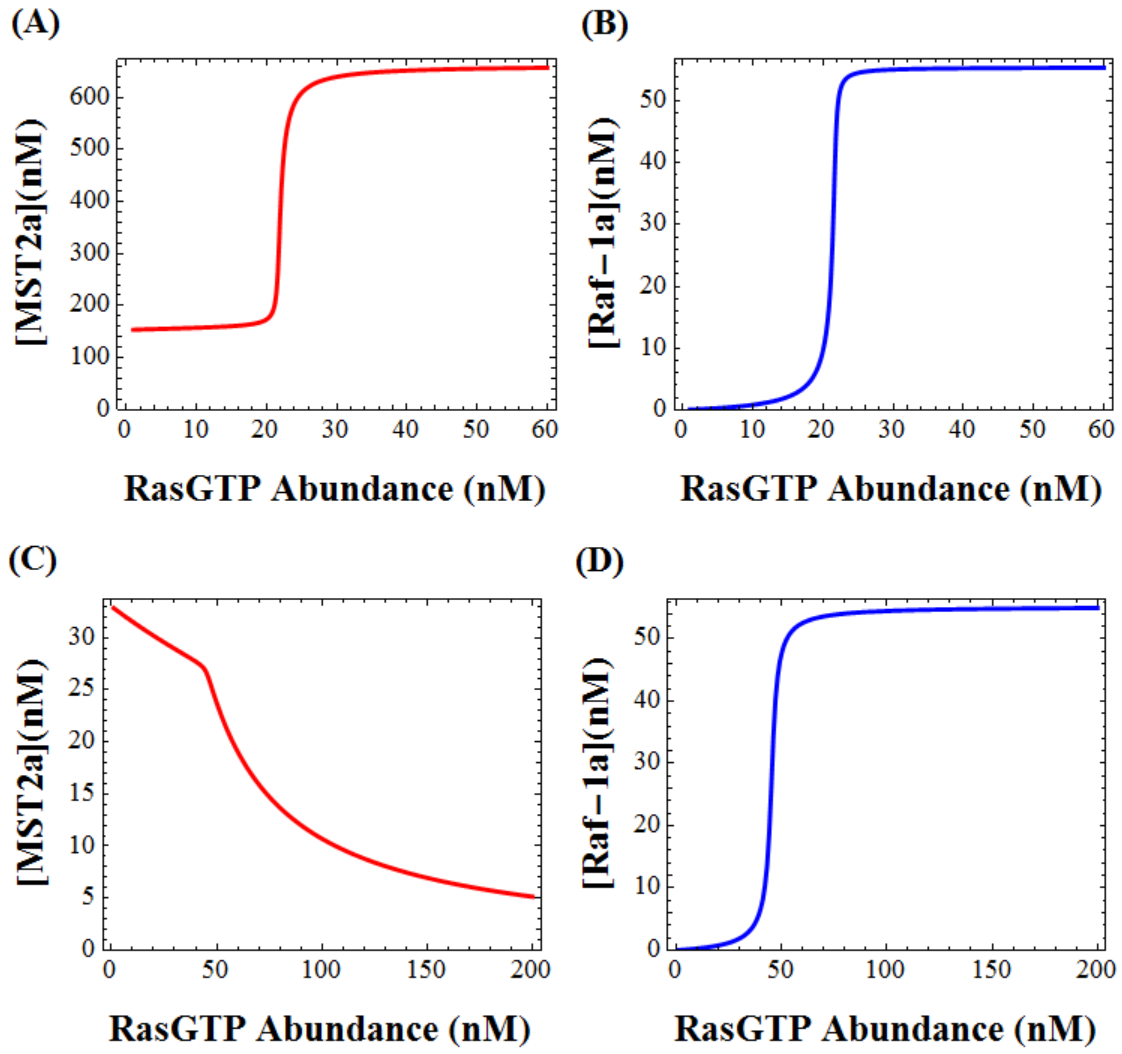

Fig. M6. Switch-like dependence of steady-state levels of active Raf-1 (Raf-1a) and active MST2 (MST2a) on the abundance of RasGTP in the elementary-step model.
(A, B) Increasing RasGTP abundance switches ON both the MST2a and Raf-1a pathways when Akt is weakly activated by RasGTP. Parameters values k_{act} = 0.001 nM^{-1}, k_{31f} = 0.0717 $nM^{-1}s^{-1}$, k_{1ar} = 0.0297 s^{-1}, k_{1b} = 0.057 s^{-1}, k_{7af} = 0.042 $nM^{-1}s^{-1}$, k_{7ar} = 0.0016 s^{-1}, k_{7b}= 0.0018 s^{-1} are used for plotting. The remaining parameter values are given in Supplementary Table 6.
(C,D) Increasing RasGTP abundance switches ON the Raf-1a pathway but switches OFF the MST2 pathway when Akt is strongly activated by RasGTP. Parameters values k_{act} = 0.1 nM^{-1}, k_{1af} = 0.0917 $nM^{-1}s^{-1}$, k_{1ar} = 0.0175 s^{-1}, k_{1b} = 0.025 s^{-1}, k_{7af} = 0.0013 $nM^{-1}s^{-1}$, k_{7ar} = 0.289 s^{-1}, k_{7b}= 0.199 s^{-1} are used for plotting. The remaining parameter values are given in Supplementary Table 6.

© 2014 Macmillan Publishers Limited. All rights reserved.

4. Modelling the effects of siRNA MST2 and LATS1-mediated feedback perturbation

4.1. Modelling the effects of increasing siRNA MST2

The experimental data shown in Fig.2B show switch-like transitions between Raf-1 – MST2 and Raf-1 – MEK complexes in cells, when one of these Raf-1 binding partners is gradually downregulated. Therefore, we simulated the siRNA MST2 knockdown in the simplified core model shown in Fig.M2A (Fig.M7). Increasing siRNA targeting MST2 induces a switch-like disassembly of Raf-1 – MST2 complex in favour of a switch-like formation of Raf-1 – MEK complexes. These simulations are fully consistent with the experimental data shown in Fig. 2B.

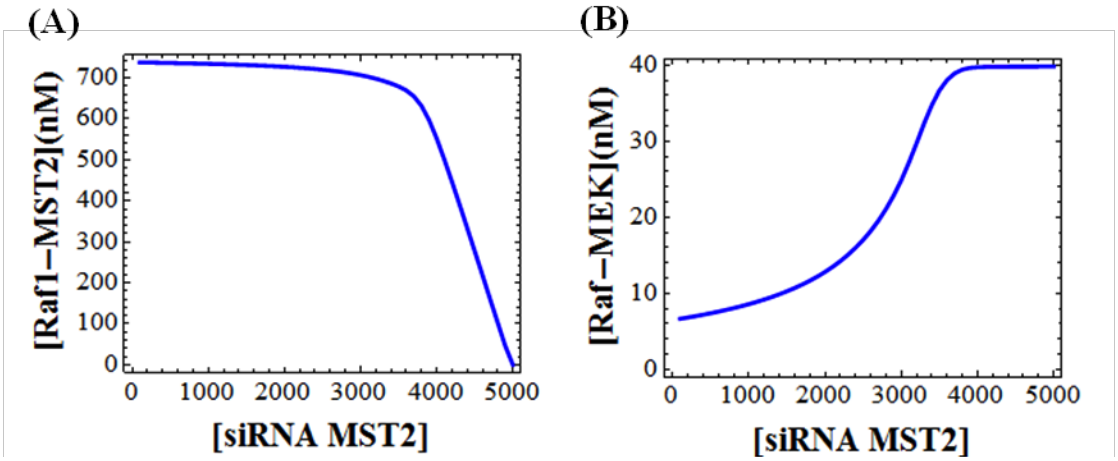

Figure M7. (A,B) Steady-state dependence of the levels of Raf-1-MST2 and Raf-1-MEK complexes on increasing level of MST2 siRNA (arbitrary unit) simulated using the extended Raf-1/MST2 model (Tables M1-3). Parameter values used for plotting are: k_{act} = 0.05 nM^{-1} and the remaining parameter values are given in Supplementary Table 3.

© 2014 Macmillan Publishers Limited. All rights reserved.

4.2. Modelling the effects of decreasing LATS1 feedback

In Supplementary Figure 3d we experimentally analyzed the effects of decreasing the LATS1 mediated feedback (using siRNA mediated downregulation of LATS1) in Hela cells on the levels of the MST2-Raf-1 complex, MEK-Raf-1 complex, inactive Raf-1 (pS259 Raf1), active Raf-1 (pS338Raf1), active MST2 (MST2a), and active ERK (ppERK). Model simulations correspond well with the experimental data and are shown below in Fig. M8.

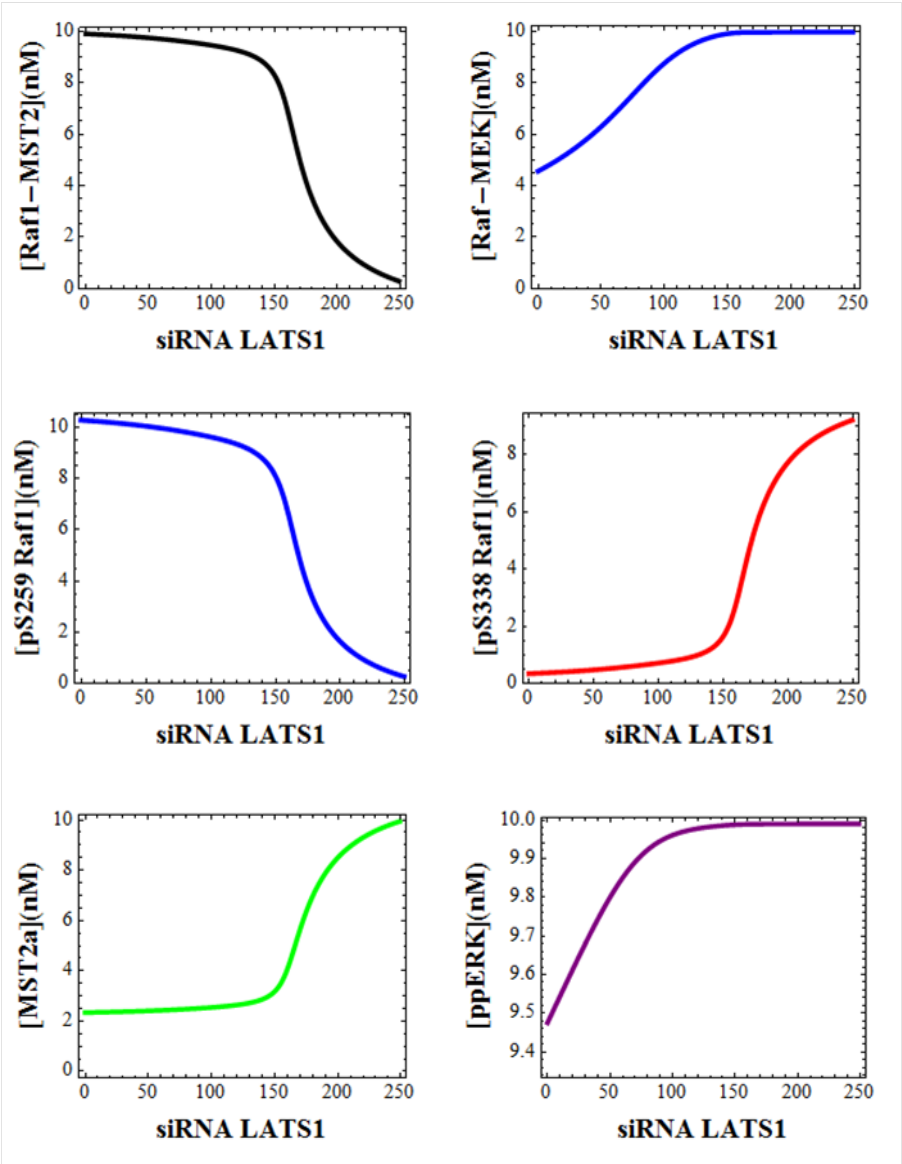

Figure M8. Steady-state dependence of the levels of various model components on increasing level of LATS1 siRNA (arbitrary unit). The dependent concentration levels are normalised to their maximum value to the range [0-10] (nM) for ease of comparison to experimental data. Parameter values used for plotting are: k_{act} = 0.0035 nM^{-1}, $K_{m1=}$ K_{m2a} = K_{m2b} = K_{m3} = K_{m4} = K_{m7} = K_{m8} = 10 nM, the remaining parameter values are given in Supplementary Table 3.

© 2014 Macmillan Publishers Limited. All rights reserved.

Supplementary References

1. O'Neill, E., Rushworth, L., Baccarini, M. & Kolch, W. Role of the kinase MST2 in suppression of apoptosis by the proto-oncogene product Raf-1. *Science (New York, N.Y.)* **306**, 2267-2270 (2004).

2. Wellbrock, C., Karasarides, M. & Marais, R. The RAF proteins take centre stage. *Nature reviews. Molecular cell biology* **5**, 875-885 (2004).

3. Matallanas, D. *et al.* Raf family kinases: old dogs have learned new tricks. *Genes Cancer* **2**, 232-260 (2011).

4. Romano, D. *et al.* Proapoptotic kinase MST2 coordinates signaling crosstalk between RASSF1A, Raf-1, and Akt. *Cancer research* **70**, 1195-1203 (2010).

5. Anand, R., Kim, A.Y., Brent, M. & Marmorstein, R. Biochemical analysis of MST1 kinase: elucidation of a C-terminal regulatory region. *Biochemistry* **47**, 6719-6726 (2008).

6. Glantschnig, H., Rodan, G.A. & Reszka, A.A. Mapping of MST1 kinase sites of phosphorylation. Activation and autophosphorylation. *The Journal of biological chemistry* **277**, 42987-42996 (2002).

7. Hwang, E. *et al.* Structural insight into dimeric interaction of the SARAH domains from Mst1 and RASSF family proteins in the apoptosis pathway. *Proceedings of the National Academy of Sciences of the United States of America* **104**, 9236-9241 (2007).

8. Avruch, J. *et al.* Rassf family of tumor suppressor polypeptides. *The Journal of biological chemistry* **284**, 11001-11005 (2009).

9. Matallanas, D. *et al.* RASSF1A elicits apoptosis through an MST2 pathway directing proapoptotic transcription by the p73 tumor suppressor protein. *Mol Cell* **27**, 962-975 (2007).

10. Guo, C. *et al.* RASSF1A is part of a complex similar to the Drosophila Hippo/Salvador/Lats tumor-suppressor network. *Current biology : CB* **17**, 700-705 (2007).

11. Hamilton, G., Yee, K.S., Scrace, S. & O'Neill, E. ATM regulates a RASSF1A-dependent DNA damage response. *Current biology : CB* **19**, 2020-2025 (2009).

12. Praskova, M., Khoklatchev, A., Ortiz-Vega, S. & Avruch, J. Regulation of the MST1 kinase by autophosphorylation, by the growth inhibitory proteins, RASSF1 and NORE1, and by Ras. *Biochem J* **381**, 453-462 (2004).

13. Guo, C., Zhang, X. & Pfeifer, G.P. The tumor suppressor RASSF1A prevents dephosphorylation of the mammalian STE20-like kinases MST1 and MST2. *The Journal of biological chemistry* **286**, 6253-6261 (2011).

14. Chan, E.H. *et al.* The Ste20-like kinase Mst2 activates the human large tumor suppressor kinase Lats1. *Oncogene* **24**, 2076-2086 (2005).

© 2014 Macmillan Publishers Limited. All rights reserved.

15. Diaz, B. *et al.* Phosphorylation of Raf-1 serine 338-serine 339 is an essential regulatory event for Ras-dependent activation and biological signaling. *Molecular and cellular biology* **17**, 4509-4516 (1997).

16. Mason, C.S. *et al.* Serine and tyrosine phosphorylations cooperate in Raf-1, but not B-Raf activation. *The EMBO journal* **18**, 2137-2148 (1999).

17. Xiang, X., Zang, M., Waelde, C.A., Wen, R. & Luo, Z. Phosphorylation of 338SSYY341 regulates specific interaction between Raf-1 and MEK1. *The Journal of biological chemistry* **277**, 44996-45003 (2002).

18. Sturm, O.E. *et al.* The mammalian MAPK/ERK pathway exhibits properties of a negative feedback amplifier. *Science signaling* **3**, ra90 (2010).

19. Markevich, N.I., Hoek, J.B. & Kholodenko, B.N. Signaling switches and bistability arising from multisite phosphorylation in protein kinase cascades. *J Cell Biol* **164**, 353-359 (2004).

20. Dougherty, M.K. *et al.* Regulation of Raf-1 by direct feedback phosphorylation. *Mol Cell* **17**, 215-224 (2005).

21. Eltis, L.D., Herbert, R.G., Barker, P.D., Mauk, A.G. & Northrup, S.H. Reduction of horse heart ferricytochrome c by bovine liver ferrocytochrome b5. Experimental and theoretical analysis. *Biochemistry* **30**, 3663-3674 (1991).

22. Koren, R. & Hammes, G.G. A kinetic study of protein-protein interactions. *Biochemistry* **15**, 1165-1171 (1976).

23. Northrup, S.H. & Erickson, H.P. Kinetics of protein-protein association explained by Brownian dynamics computer simulation. *Proceedings of the National Academy of Sciences of the United States of America* **89**, 3338-3342 (1992).

24. Nakakuki, T. *et al.* Ligand-specific c-Fos expression emerges from the spatiotemporal control of ErbB network dynamics. *Cell* **141**, 884-896 (2010).

25. Schoeberl, B., Eichler-Jonsson, C., Gilles, E.D. & Muller, G. Computational modeling of the dynamics of the MAP kinase cascade activated by surface and internalized EGF receptors. *Nat Biotechnol* **20**, 370-375 (2002).

© 2014 Macmillan Publishers Limited. All rights reserved.